

NASA TECHNICAL NOTE



NASA TN D-8091

NASA TN D-8091



·LOAN COPY· RETURN TO  
AFWL TECHNICAL LIBRARY  
·KIRTLAND AFB, N. M.

UPWASH ANGLES NEAR  
ENGINE INLETS OF  
AN EXTERNALLY BLOWN  
FLAP STOL TRANSPORT

*Roger L. Naeseth*

*Langley Research Center*

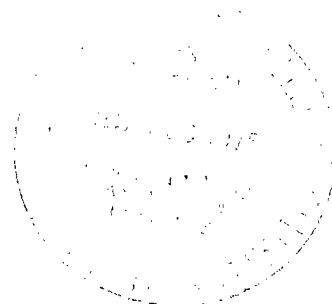
*and*

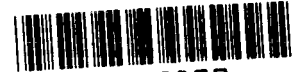
*Danny R. Hoad*

*Langley Directorate*

*U.S. Army Air Mobility R&D Laboratory*

*Hampton, Va. 23665*





0133809

1. Report No. NASA TN D-8091	2. Government Accession No.	3. Rec., ... Category No.	
4. Title and Subtitle UPWASH ANGLES NEAR ENGINE INLETS OF AN EXTERNALLY BLOWN FLAP STOL TRANSPORT	5. Report Date November 1975		6. Performing Organization Code
	7. Author(s) Roger L. Naeseth, Langley Research Center; and Danny R. Hoad, Langley Directorate, U.S. Army Air Mobility R&D Laboratory		8. Performing Organization Report No. L-10406
9. Performing Organization Name and Address NASA Langley Research Center Hampton, Va. 23665	10. Work Unit No. 505-10-31-02		11. Contract or Grant No.
	12. Sponsoring Agency Name and Address National Aeronautics and Space Administration Washington, D.C. 20546		13. Type of Report and Period Covered Technical Note
15. Supplementary Notes	14. Sponsoring Agency Code		
16. Abstract  <p>An investigation has been conducted in the Langley V/STOL tunnel to determine the upwash flow angles in the region of the nacelle inlets of a representative powered-lift transport configuration operating at high lift coefficients. The upwash angles were indicated by tufts and measured from photographs. A potential-flow program was used to estimate these flow angles.</p> <p>Large upflow angles exist near the inlets of the nacelles; the highest value (<math>67.3^\circ</math>) occurred with flaps at <math>15^\circ, 35^\circ, 55^\circ</math>, an angle of attack of <math>25.7^\circ</math>, and a thrust coefficient of 4. The upflow angle was found to be strongly dependent on the circulation lift, regardless of the flap deflection, angle of attack, or thrust coefficient used to generate this circulation lift. The potential-flow calculations away from the nacelle inlets agreed fairly well with the experimental data.</p>			
17. Key Words (Suggested by Author(s)) Powered lift Upwash angles Engine inlets STOL		18. Distribution Statement Unclassified - Unlimited  Subject Category 02	
19. Security Classif. (of this report) Unclassified	20. Security Classif. (of this page) Unclassified	21. No. of Pages 47	22. Price* \$3.75

# UPWASH ANGLES NEAR ENGINE INLETS OF AN EXTERNALLY BLOWN FLAP STOL TRANSPORT

Roger L. Naeseth  
Langley Research Center

and Danny R. Hoad  
Langley Directorate, U.S. Army Air Mobility R&D Laboratory

## SUMMARY

An investigation has been conducted in the Langley V/STOL tunnel to determine the upwash flow angles in the region of the nacelle inlets of a representative powered-lift transport configuration operating at high lift coefficients. The upwash angles were indicated by tufts and measured from photographs. A potential-flow program was used to estimate these flow angles.

Large upflow angles exist near the inlets of the nacelles; the highest value ( $67.3^{\circ}$ ) occurred with flaps at  $15^{\circ}$ ,  $35^{\circ}$ ,  $55^{\circ}$ , an angle of attack of  $25.7^{\circ}$ , and a thrust coefficient of 4. The upflow angle was found to be strongly dependent on the circulation lift, regardless of the flap deflection, angle of attack, or thrust coefficient used to generate this circulation lift. The potential-flow calculations away from the nacelle inlets agreed fairly well with the experimental data.

## INTRODUCTION

An aircraft capable of efficient cruise performance and also short take-off and landing (STOL) would generally have a powered high-lift system. This lift system, in developing lift coefficients approaching 10, induces large upwash angles in front of the wing in the region of the nacelles. These flow fields must be defined in order that the nacelles can be properly designed to minimize flow distortion at the engine face.

Some theoretical work has been done to calculate the flow field using two-dimensional potential flow (ref. 1) and two-dimensional flow modified to include three-dimensional effects (ref. 2). Little experimental work has been made available for design and comparison with calculated values of the flow field associated with the high lift coefficient generated by STOL aircraft. Maximum upwash angles for conventional take-off and landing (CTOL) transport aircraft are near  $10^{\circ}$  (ref. 3). STOL aircraft producing very high lift coefficients

generate upwash angles of the order of  $50^{\circ}$ ; therefore, the engine-inlet flow distortion is much more severe for a STOL aircraft.

In the present investigation flow angles were measured at two spanwise stations in the vicinity of the nacelles of a four-engine externally blown flap STOL transport model by reading photographs of a tuft grid placed streamwise and adjacent to the engine nacelles. Theoretical estimates of the upwash angle were made by computing the wing circulation distribution with the vortex-lattice method of reference 4 and then evaluating the flow field from a modified version of this vortex-lattice method.

Diagrams of the flow fields determined from the test photographs for landing and take-off flap deflections are presented. Test conditions included a range of thrust coefficient from 0 to 4.0 and a range of lift coefficient from 1.9 to 9.3. Estimated values of up-flow angles are compared to the experimentally determined values.

## SYMBOLS

The values in this paper are given in both SI and U.S. Customary Units. Measurements and calculations were made in U.S. Customary Units. Factors relating these units are given in reference 5.

b	wing span, 1.90 m (6.25 ft)
$C_L$	tail-off lift coefficient, $\frac{\text{Lift}}{qS}$
$C_{L,\Gamma}$	thrust-removed (circulation) lift coefficient, $C_L - \eta C_\mu \sin(\alpha + \delta_j)$
$C_\mu$	thrust coefficient, $\frac{\text{Static thrust}}{qS}$
$\bar{c}$	mean geometric chord, m (ft)
$F_A$	axial force, N (lb)
$F_N$	normal force, N (lb)
q	free-stream dynamic pressure, Pa (lb/ft <sup>2</sup> )
R	radius of upper half of nacelle, $0.065 \frac{b}{2}$
S	wing area, m <sup>2</sup> (ft <sup>2</sup> )

V	free-stream velocity, m/sec (ft/sec)
X,Y	axes used for wing planform definition
x,y	coordinates of breakpoints of wing planform, x positive forward and y positive toward right wing, cm (in.)
x/c	fraction of projected wing chord (slats and flaps included)
$\frac{y}{b/2}$	tuft grid location, fraction of semispan
z	vertical location of grid relative to wing-chord plane, m (ft)
$\alpha$	angle of attack, deg
$\delta_f$	flap deflection, positive trailing edge down, deg
$\delta_j$	jet-exhaust deflection angle, $\text{arc tan } \frac{F_N}{F_A}$ , deg
$\eta$	flap turning efficiency, $\frac{\sqrt{F_N^2 + F_A^2}}{\text{Thrust}}$
$\theta$	local upflow angle, measured with respect to model horizontal axis, deg
$\phi$	local upwash angle, measured with respect to free stream, deg

### MODEL AND APPARATUS

The model was a typical powered-lift configuration equipped with externally blown, triple-slotted flaps. Geometric characteristics of the model are given in figure 1. Photographs of the model installed in the Langley V/STOL tunnel with tail on are presented in figure 2. The model had full-span flaps which were deflected to represent the take-off and landing configurations (fig. 3). The series of numbers which designate the trailing-edge flap deflections are for the three elements of the flap system.

A large chord slat, set at a deflection of  $50^\circ$ , was used in conjunction with the flaps. For some tests, wood fillers were installed to close the gap between the slat and the nacelles. One of the fillers can be seen in figure 2 at the inboard end of the outboard slat.

The four nacelles installed on the model were located below and forward of the wing. The exhaust flow of the high-bypass-ratio engines were simulated by two-part ejectors using compressed air. The details of these ejectors are presented in reference 6. Further geometric characteristics of this model can be found in reference 7.

The frame for the tuft grid used to indicate the flow angles ahead of the wing was constructed of steel rods and bolted to the outboard sides of the port nacelles. The grid was constructed in units of  $R$ , which is the radius of the upper half of the nacelle (fig. 4). Wire standoff masts were used to decrease the interference of the supporting frame. In addition, four long tufts were installed on masts long enough to put the tufts on the vertical plane of the center line of the nacelle inlet and were used only during the landing configuration tests. The tuft locations are presented in figure 4.

## TEST AND PROCEDURES

This investigation was conducted in the Langley V/STOL tunnel at a nominal free-stream dynamic pressure of 479 Pa (10 lb/ft<sup>2</sup>) for a Reynolds number of  $0.54 \times 10^6$ , based on the wing mean geometric chord of 27.81 cm (10.95 in.). For this investigation the horizontal tail was off. Most of the tests were made over an angle-of-attack range of  $0^\circ$  to  $25^\circ$  for static thrust coefficients of 0, 2, and 4. The various thrust levels were obtained by setting the primary air-supply pressure at the model plenum in accordance with a previously determined relationship between model plenum pressure and model thrust.

Force and flow-angle measurements were made at selected angles of attack and thrust coefficients. A complete investigation had already been conducted to determine the longitudinal aerodynamics of this model (ref. 7). Maximum angle-of-attack corrections due to wind-tunnel wall effects were determined to be approximately  $0.5^\circ$  in reference 7; therefore, no corrections to these data have been made.

Flow-angle data were recorded by a camera for the landing and take-off configurations at  $C_\mu = 0, 2, \text{ and } 4$  and three angles of attack (near zero, midway to stall, and just below stall). Test conditions and configurations are listed in table I. The angle of each tuft was measured relative to the body axis on the photograph. An example of the photographs taken is presented in figure 5.

## PRESENTATION OF RESULTS

The tail-off lift-coefficient characteristics of the model which pertain to this investigation are presented in figure 6. These data were obtained from reference 7.

The experimental data are presented in tuft grid form, as measured, in figures 7 to 13. The lift coefficients presented were obtained for the tail-off configuration from ref-

erence 7. The nacelles are outlined on the figures to show their location relative to the grid. The upflow angle  $\theta$  is given at each tuft location.

A summary of the upwash angle  $\phi$  for one tuft is presented in figure 14 as a function of thrust-removed lift coefficient. The geometric characteristics required as input for the program in reference 4 are presented in figure 15.

Comparisons of experimental and calculated results, arranged in essentially a grid form, are presented in figures 16 to 22.

## DISCUSSION

### Basic Data

The data of figures 7 to 13 show large effects of the wing and engine thrust on the flow field in the vicinity of the nacelles. The upflow angle increased as  $C_L$  was increased by increasing  $\alpha$  (for example, see figs. 8(a), 8(b), and 8(c)). The upflow angle increased as  $C_L$  was increased by increasing  $C_{\mu}$  (for example, see figs. 7 to 9). Increasing  $C_{\mu}$  from 0 to 2 had a large effect, but a further increase to 4 had much less effect. The maximum value of upflow angle ( $67.3^\circ$ ) occurred at a position ahead of the lower lip of the nacelle at a lift coefficient of 9.33, a thrust coefficient of 4.0, and angle of attack of  $25.7^\circ$  (fig. 12(c)).

The long tuft mounted on the outboard inlet centerline indicated higher upflow angles for the power-off condition (fig. 10(c)) than those indicated for power-on conditions (figs. 11(b) and 12(b)). The effect (local induced upflow angle due to nacelle flow) would likely be greater (that is the upflow angle would be even smaller) if the flow into the inlet was of the order of the scaled value. The ejector nacelles produce scaled thrust values but produce only approximately one-half of the scaled inlet mass flow. The long tufts below the nacelle centerline indicate very large upflow angles (increasing with power), which could create large engine-face distortion problems.

A summary plot showing the variation with thrust-removed lift coefficient of the upwash angle  $\phi$  between nacelles indicated by one tuft, which is located a distance  $R$  behind the leading edge of the inboard nacelle and on the horizontal plane through the centerline of the inboard nacelle, is presented in figure 14. The thrust-removed lift coefficients, which were computed by subtracting the direct-thrust component of lift from the overall lift coefficient, are presented in table II. The figure indicates that, for power-on conditions, the variation of upwash angle  $\phi$  with circulation lift coefficient is essentially the same for different thrust coefficients and flap deflections.

### Prediction Calculations

The lift developed by a powered-lift system can be separated into three parts according to the source of the lift: (1) the lift that was produced by the unpowered wing, (2) the

lift due to the component of the jet which has been redirected by the flap system, and (3) the lift due to circulation induced by power. Experimental results indicated that the upwash angle ahead of the wing could be estimated based on thrust-removed lift coefficient.

The thrust-removed lift coefficient (circulation lift coefficient) and wing geometric characteristics were input into the program described in reference 4 to determine the magnitude of circulation.

The geometry required included planform breakpoints, locations of intersections of lines defining the planform (fig. 15), and the chordwise angle-of-attack distribution to represent the slat and flaps on the wing. The program did not account for thickness effects, so the wing section geometry was reduced to a camber line represented by straight lines (fig. 3). Experience with the program in reference 4 indicated that a choice of 10 chordwise vortices equally spaced was a reasonably good representation of the high-lift system, since the planform definition points, as shown in figure 15, could be placed in approximately the right places chordwise without modification of the program. Reference 4 indicates that 20 spanwise stations are adequate. The local angle of attack and circulation were extracted from the program of reference 4 and input into a flow-field program, derived from the vortex-lattice method, to compute the upwash angle ahead of the wing. The experimental angle of attack was then added to the upwash angle to obtain the total upflow angle  $\theta$ .

### Calculated Results

The calculated results are compared to experimental results in figures 16 to 22. The method of calculation appears to be useful, showing fair agreement in the regions away from the nacelle inlet. The calculations near the nacelle inlet are lower than the experimentally measured angles. The program does not include the geometry of the large nacelles or the sink created by the mass flow into the nacelle when powered. These effects must be considered to properly simulate the flow near the nacelles. The calculations for the upflow angle  $\theta$  outboard of the nacelles agree very well with the experimental data (fig. 22).

### CONCLUDING REMARKS

An investigation has been conducted to determine the upwash flow angles in the region of the nacelle inlets of a representative powered-lift transport configuration operating at high lift coefficients. The upwash angles were indicated by tufts and angles measured from photographs. A potential-flow program was used to estimate these flow angles as a comparison.

The results of the investigation indicate that large upflow angles, as high as  $67.3^{\circ}$ , exist near the inlets of nacelles located forward and below a wing configured for externally blown flaps. The highest value occurred with flaps deflected for landing at a  $25.7^{\circ}$  angle of attack and a thrust coefficient of 4.

The upwash angle was found to be strongly dependent on the circulation or thrust-removed lift, regardless of flap deflection, angle of attack, or thrust coefficient used to generate this circulation lift.

The results of calculations made by a potential-flow method indicated that calculated upflow angles were in fair agreement with experimental values except near the nacelle inlets. The nacelle geometry and sink created by the mass flow into the nacelle when powered must be considered to properly simulate the flow near the nacelle. Calculated upflow angles outboard of the nacelles were in good agreement.

Langley Research Center  
National Aeronautics and Space Administration  
Hampton, Va. 23665  
October 8, 1975

#### REFERENCES

1. Albers, James A.; and Potter, Merle C.: Potential Flow Solution for a STOL Wing Propulsion System. NASA TN D-6394, 1971.
2. Albers, James A.: Predicted Upwash Angles at Engine Inlets for STOL Aircraft. NASA TM X-2593, 1972.
3. Douglass, W. M.: Aerodynamic Installation of High-Bypass-Ratio Fan Engines. [Preprint] 660732, Soc. Automot. Eng., Oct. 1966.
4. Margason, Richard J.; and Lamar, John E.: Vortex-Lattice FORTRAN Program for Estimating Subsonic Aerodynamic Characteristics of Complex Planforms. NASA TN D-6142, 1971.
5. Mechtly, E. A.: The International System of Units - Physical Constants and Conversion Factors (Second Revision). NASA SP-7012, 1973.
6. Hoad, Danny R.: Longitudinal Aerodynamic Characteristics of an Externally Blown Flap Powered-Lift Model With Several Propulsive System Simulators. NASA TN D-7670, 1974.
7. Gentry, Garl L., Jr.: Wind-Tunnel Investigation of an Externally Blown Flap STOL Transport Model Including an Investigation of Wall Effects. NASA TM X-3009, 1974.

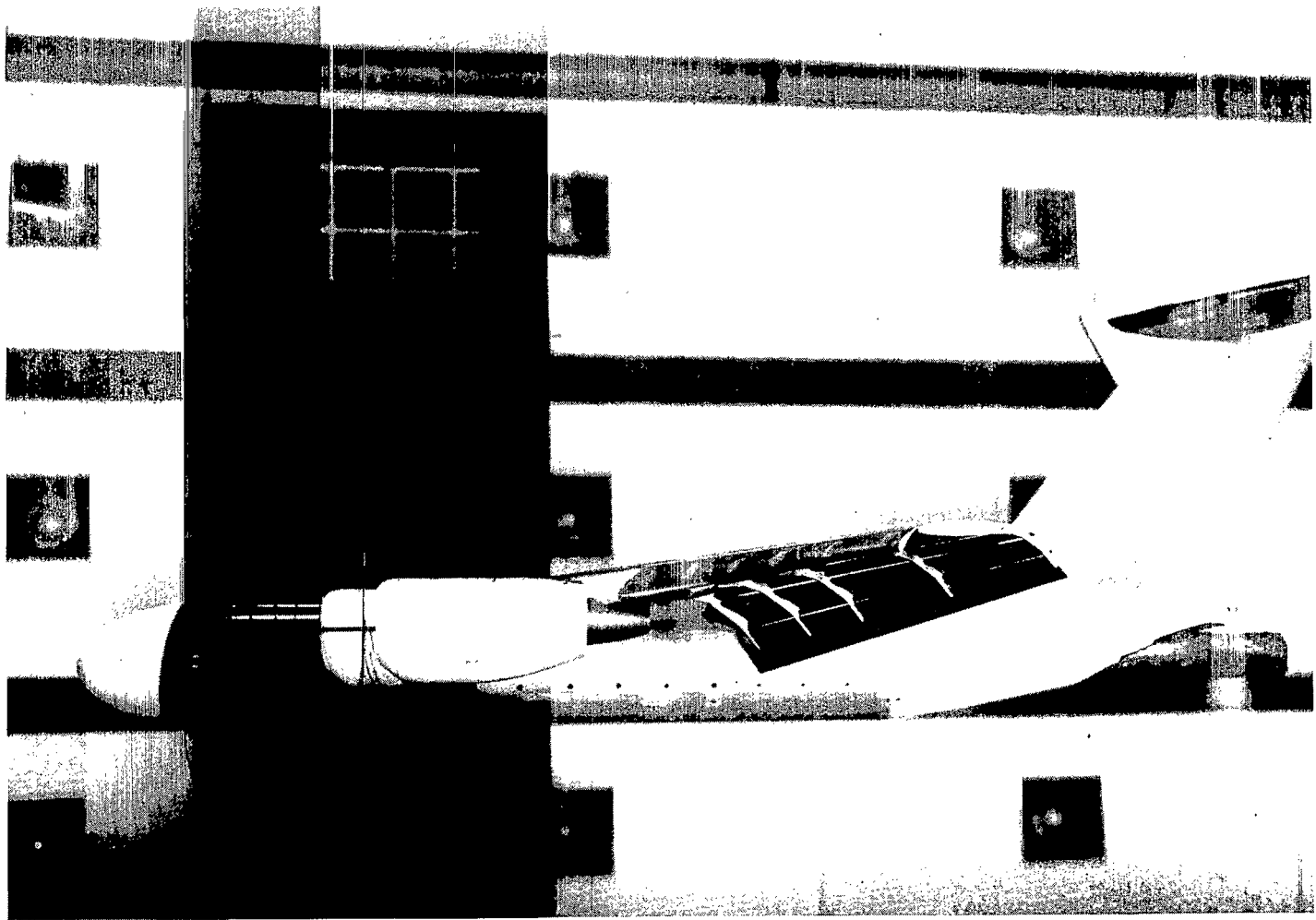
TABLE I. - TEST CONDITIONS AND CONFIGURATIONS

Figure presenting -		Grid location, $y/(b/2)$	Flap setting, deg	Slat fillers	$C_{\mu}$	$\alpha$ , deg
Flow data	Calculated results					
7	16	0.338	0,20,40	On	0	0.5, 6.6, and 12.5
8	17	.338	0,20,40	On	2.0	0.5, 12.7, and 24.8
9	18	.338	0,20,40	On	4.0	0.6, 12.7, and 24.8
10	19	.338	15,35,55	Off	0	0.5, 6.7, and 12.8
11	20	.338	15,35,55	Off	2.0	0.9, 12.4, and 25.7
12	21	.338	15,35,55	Off	4.0	1.4, 13.5, and 25.7
13	22	.502	15,35,55	On	0	-0.8, 9.0, and 17.1

TABLE II. - SUMMARY OF DIRECT THRUST  
CONTRIBUTION CALCULATIONS

$C_{\mu}$	$\alpha$ , deg	$\delta_j$ , deg	$\eta$	$C_L$	$C_{L,\Gamma}$
Take-off flaps					
2.0	0.5	22.76	0.8755	2.93	2.24
2.0	12.7	22.76	.8755	5.00	3.98
2.0	24.8	22.76	.8755	6.25	4.96
4.0	.6	20.66	.8903	3.56	2.27
4.0	12.7	20.66	.8903	5.90	3.94
4.0	24.8	20.66	.8903	7.90	5.36
Landing flaps					
2.0	0.9	44.53	0.7819	4.90	3.79
2.0	12.4	44.53	.7819	6.72	5.41
2.0	25.7	44.53	.7819	6.75	5.28
4.0	1.4	42.45	.7935	6.00	3.80
4.0	13.5	42.45	.7935	8.40	5.77
4.0	25.7	42.45	.7935	9.33	6.39

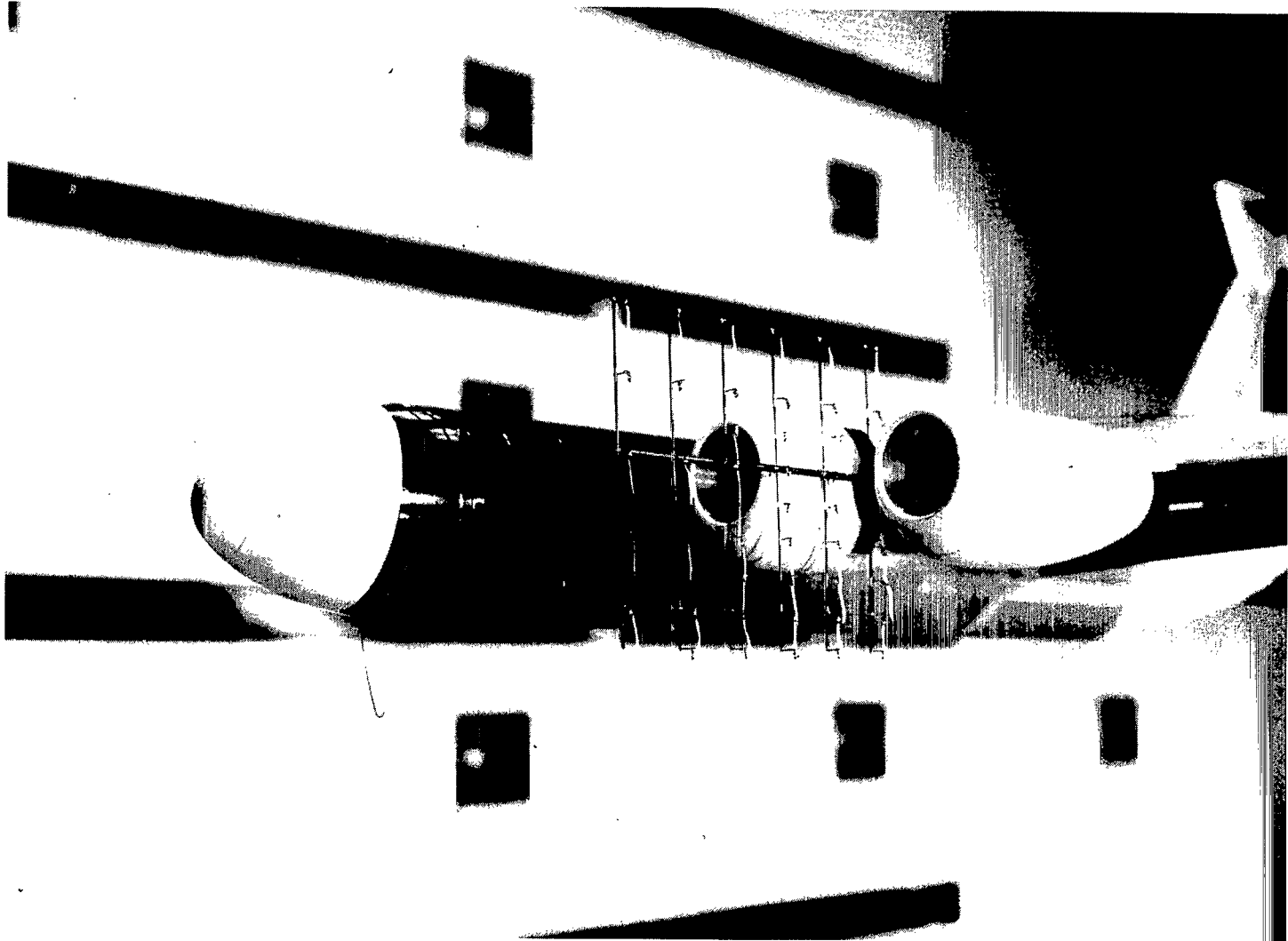




L-72-3529

(a) Side view.

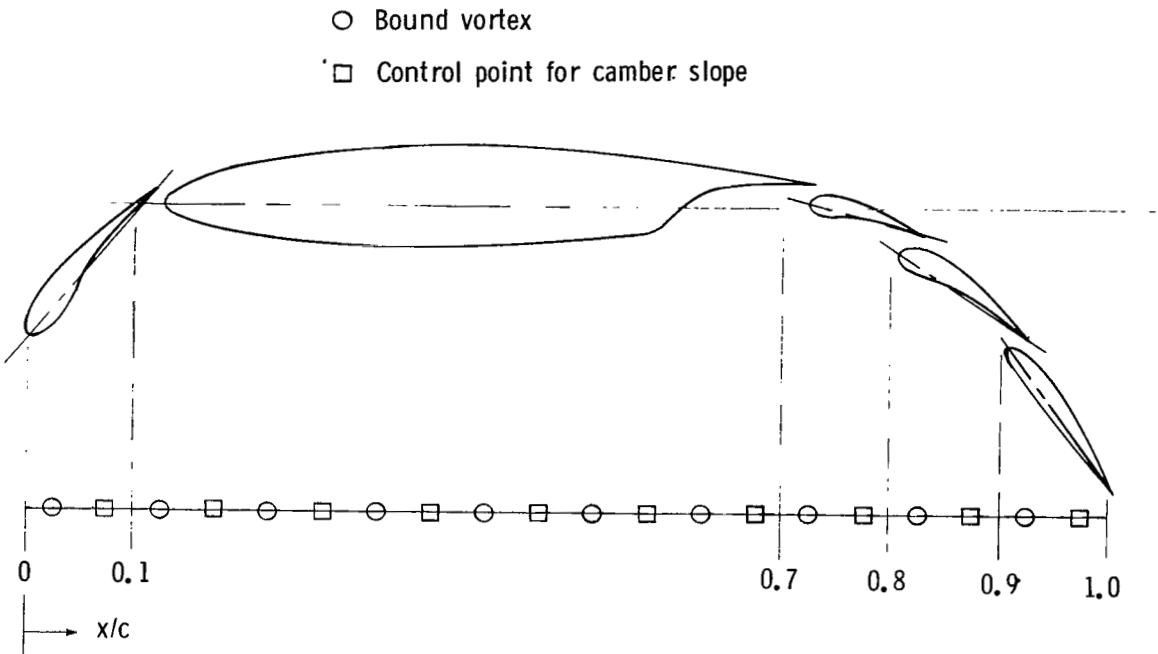
Figure 2.- Tuft grid mounted between nacelles of STOL model.  $50^\circ$  slats with fillers and flaps at  $15^\circ, 35^\circ, 55^\circ$ .



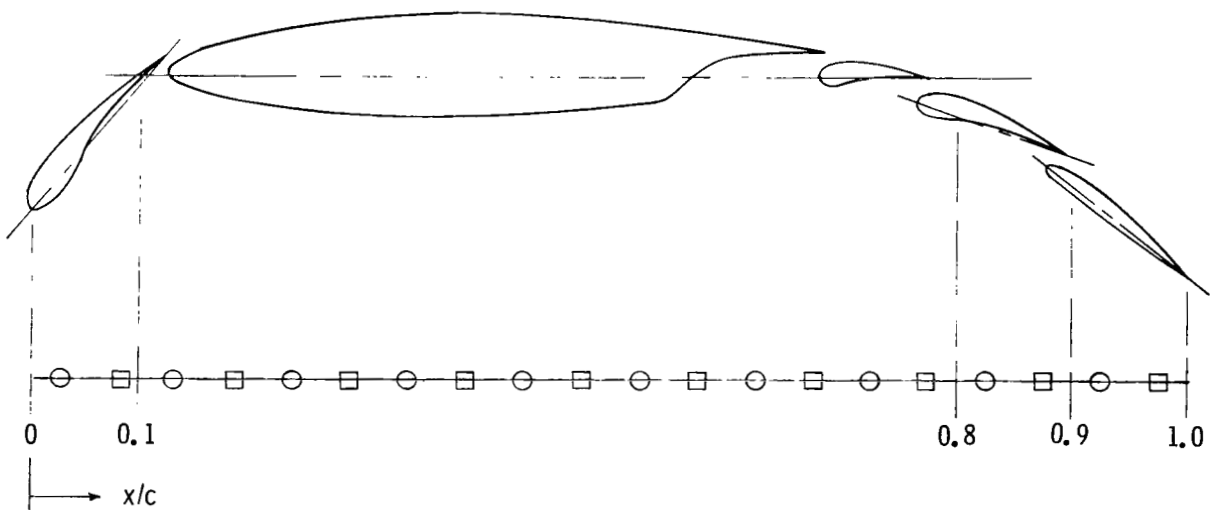
(b) Front quarter view.

Figure 2.- Concluded.

L-72-3527

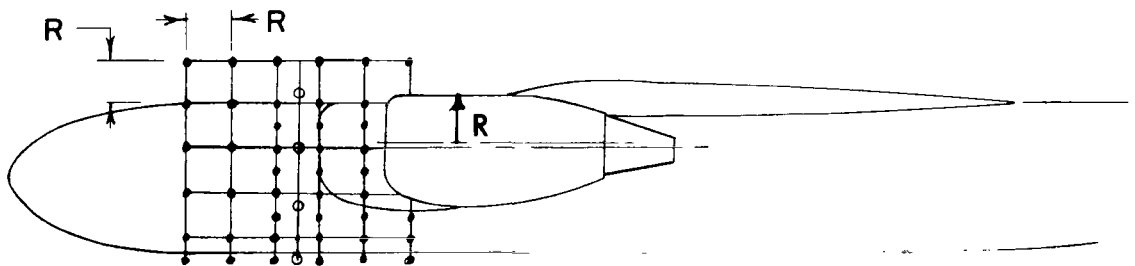
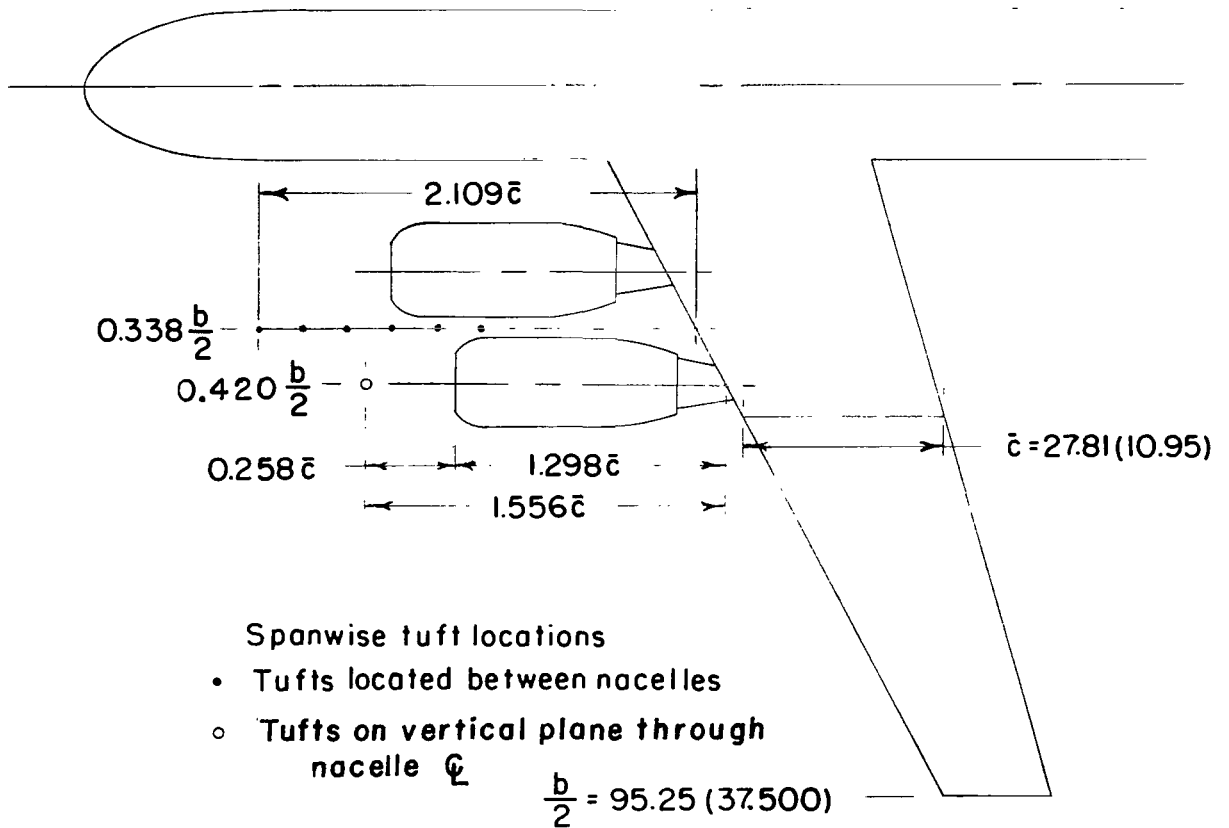


(a) Landing configuration.  $15^\circ, 35^\circ, 55^\circ$  flap deflection and  $50^\circ$  slat deflection.



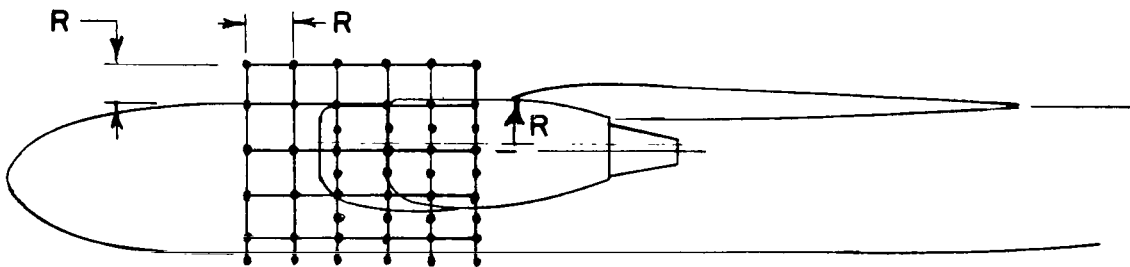
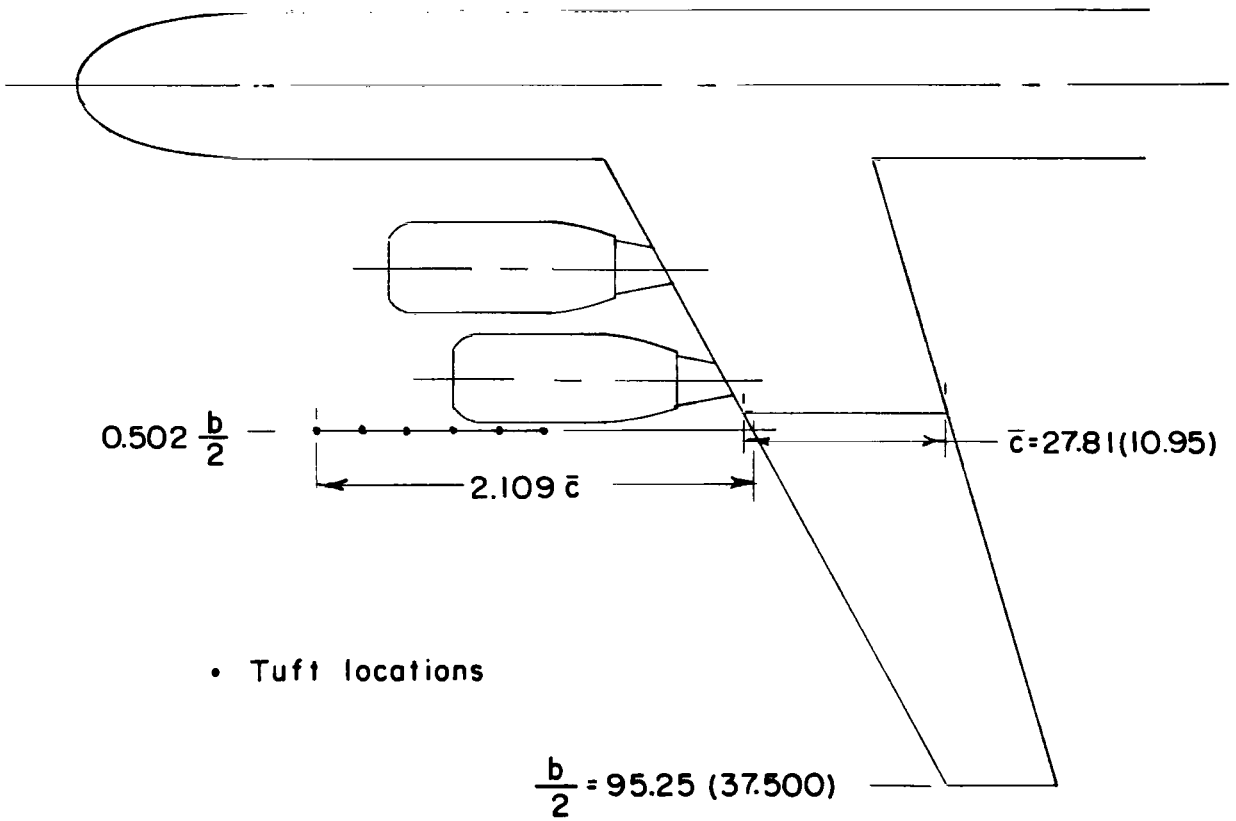
(b) Take-off configuration.  $0^\circ, 20^\circ, 40^\circ$  flap deflection and  $50^\circ$  slat deflection.

Figure 3.- Comparison of flapped wing sections and vortex-lattice representations used in calculations.



(a)  $0,338 \frac{b}{2}$  location.

Figure 4.- Location of tufts. Dimensions are in cm (in.) unless otherwise noted.

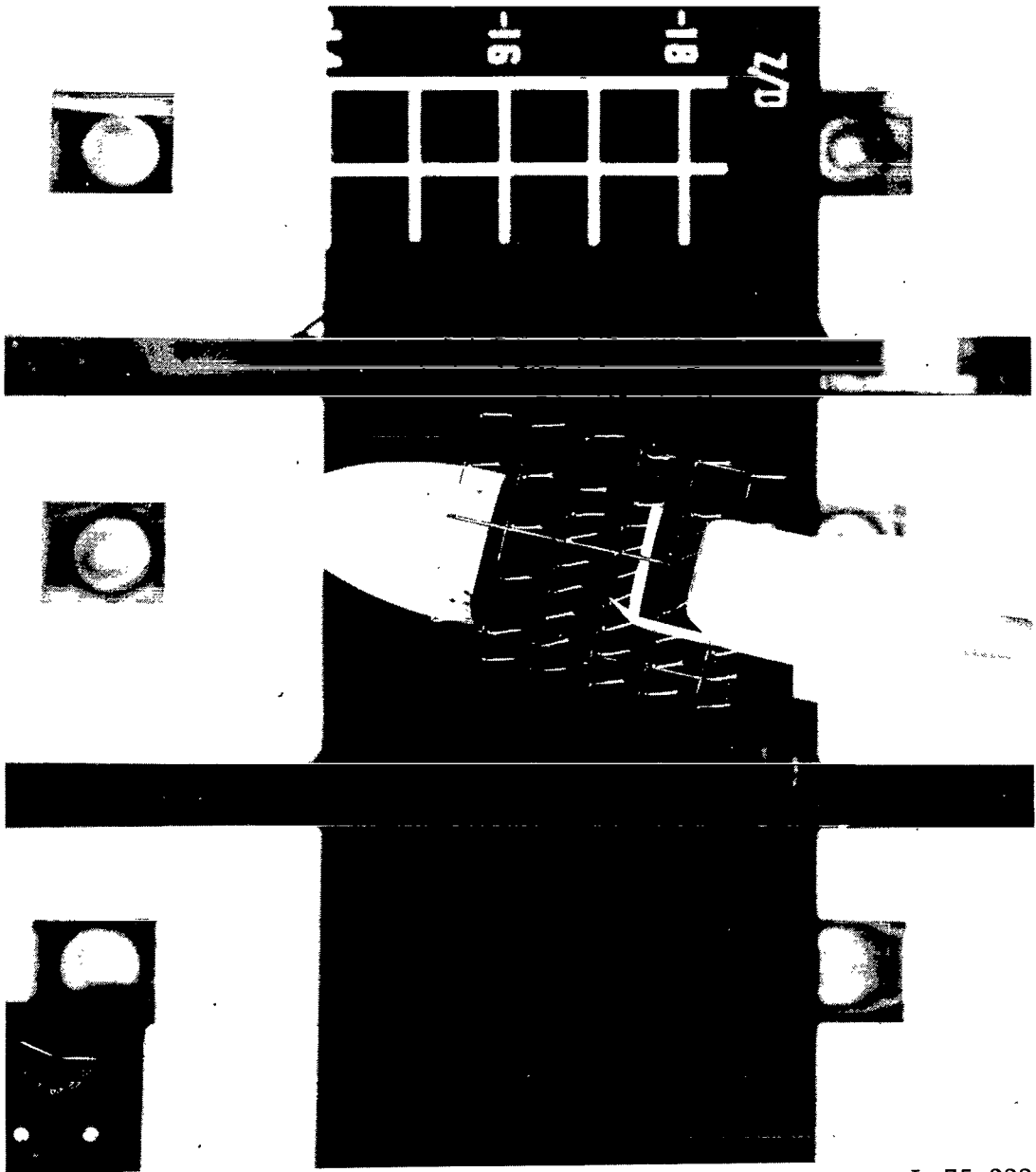


Tuft spacing = Radius of upper part of nacelle

$$R = 0.065 \frac{b}{2}$$

(b)  $0.502 \frac{b}{2}$  location.

Figure 4.- Concluded.



L-75-222

Figure 5.- Example of tuft photographs. Tuft grid located at  $0.338 \frac{b}{2}$ ; flaps at  $0^{\circ}, 20^{\circ}, 40^{\circ}$ ;  $C_{\mu} = 4.0$ ; slat fillers on.

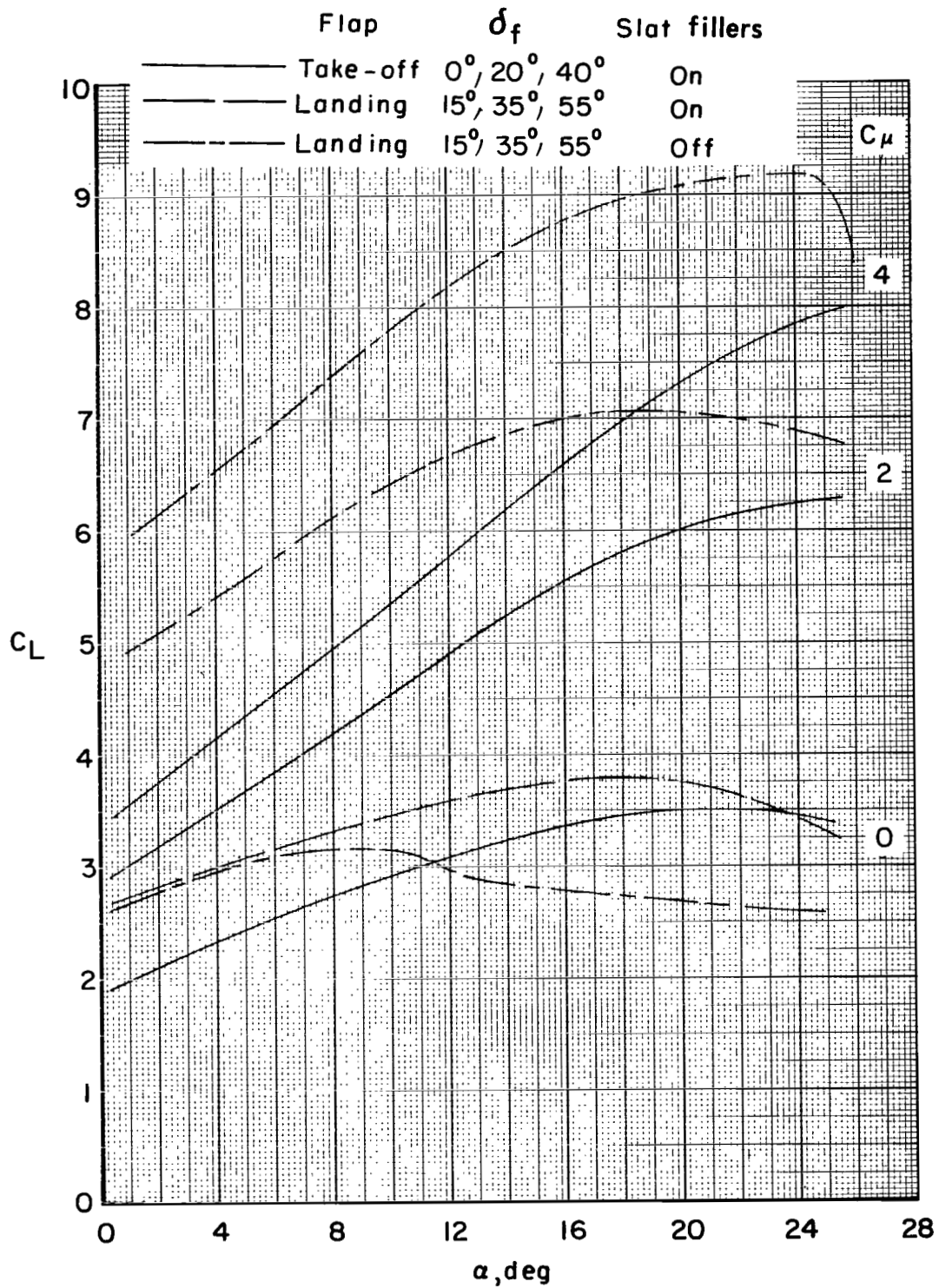
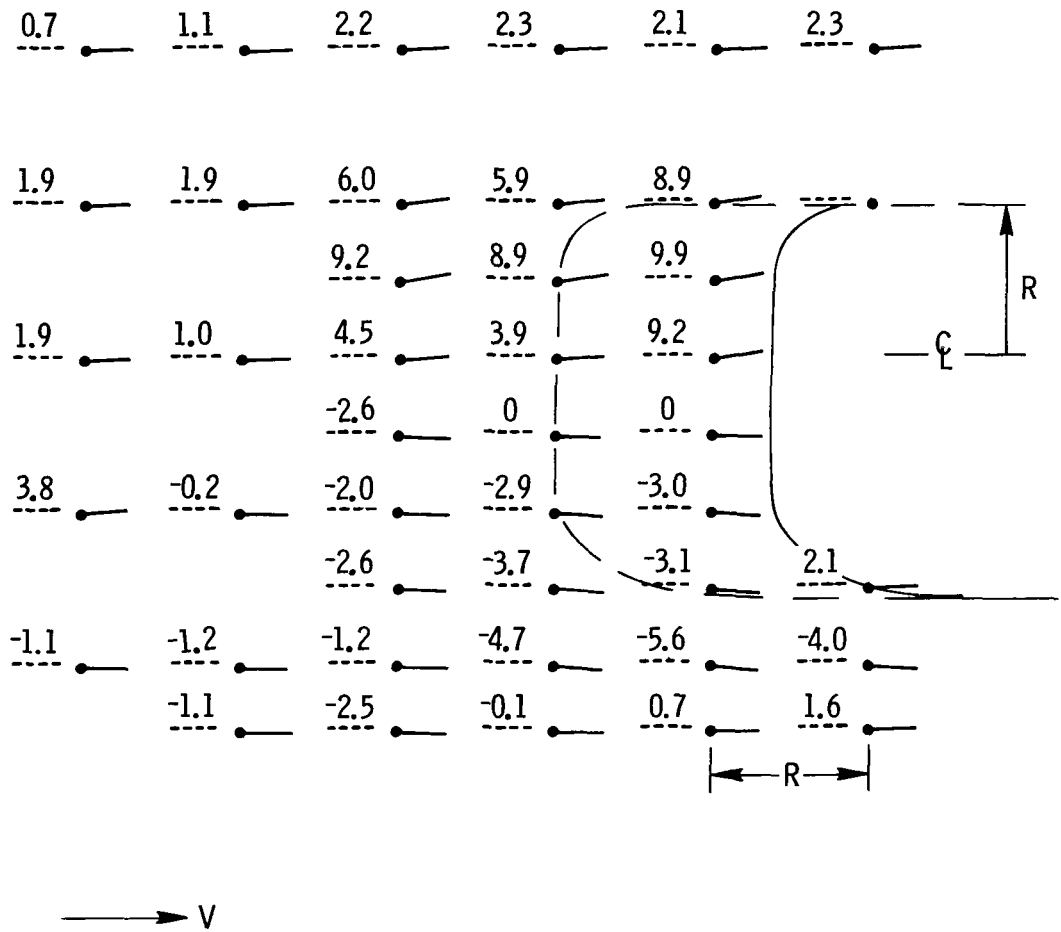


Figure 6.- Tail-off lift characteristics.

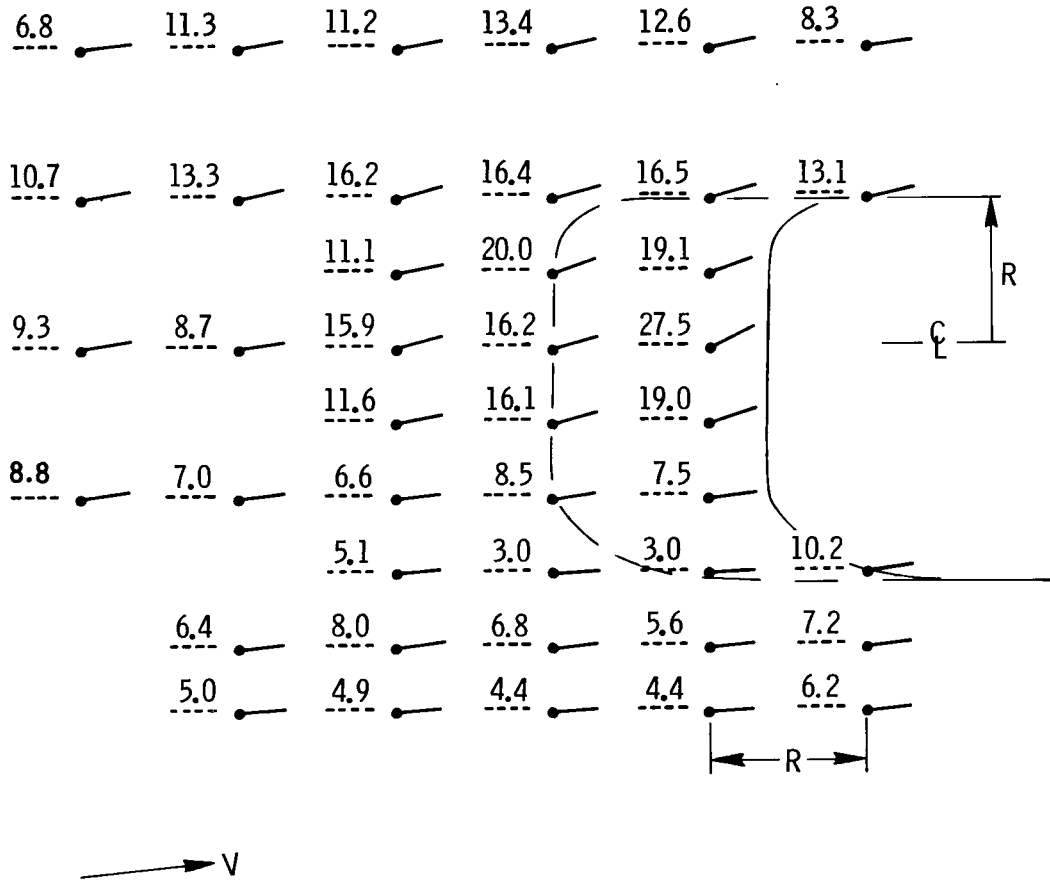
- Tufts in a chordwise plane located between the port nacelles



(a)  $\alpha = 0.5^\circ$ ;  $C_L = 1.90$ .

Figure 7.- Upflow angle, deg, between nacelles as shown by a tuft grid located at  $0.338 \frac{b}{2}$ . Flaps at  $0^\circ, 20^\circ, 40^\circ$ ;  $C_\mu = 0$ ; slat fillers on.

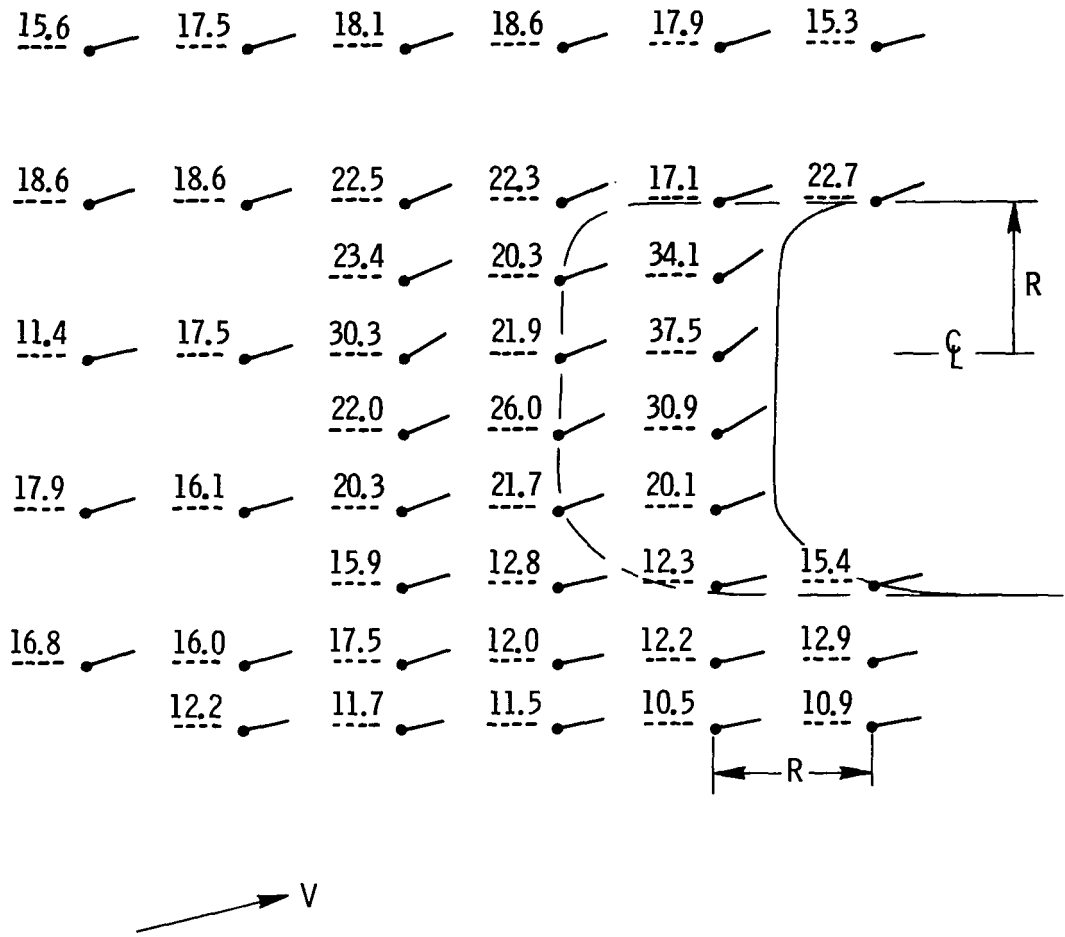
- Tufts in a chordwise plane located between the port nacelles



(b)  $\alpha = 6.6^\circ$ ;  $C_L = 2.60$ .

Figure 7.- Continued.

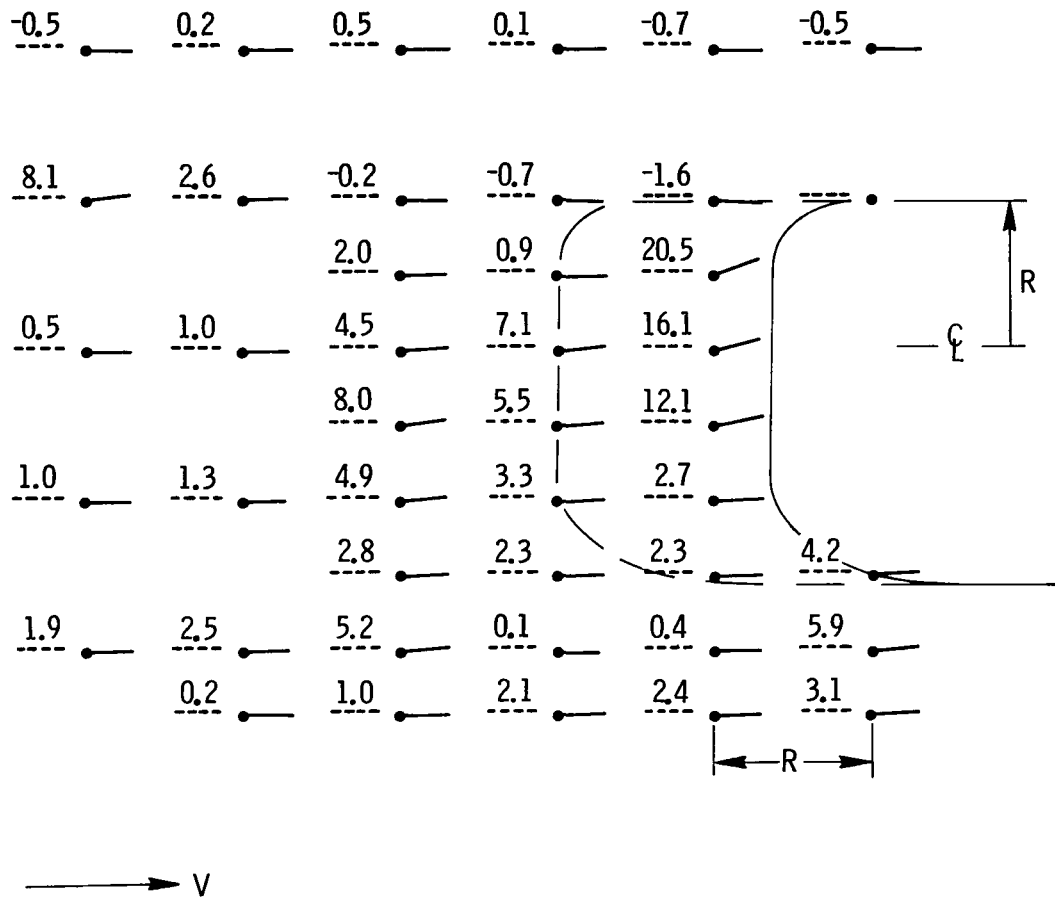
- Tufts in a chordwise plane located between the port nacelles



(c)  $\alpha = 12.5^\circ$ ;  $C_L = 3.10$ .

Figure 7.- Concluded.

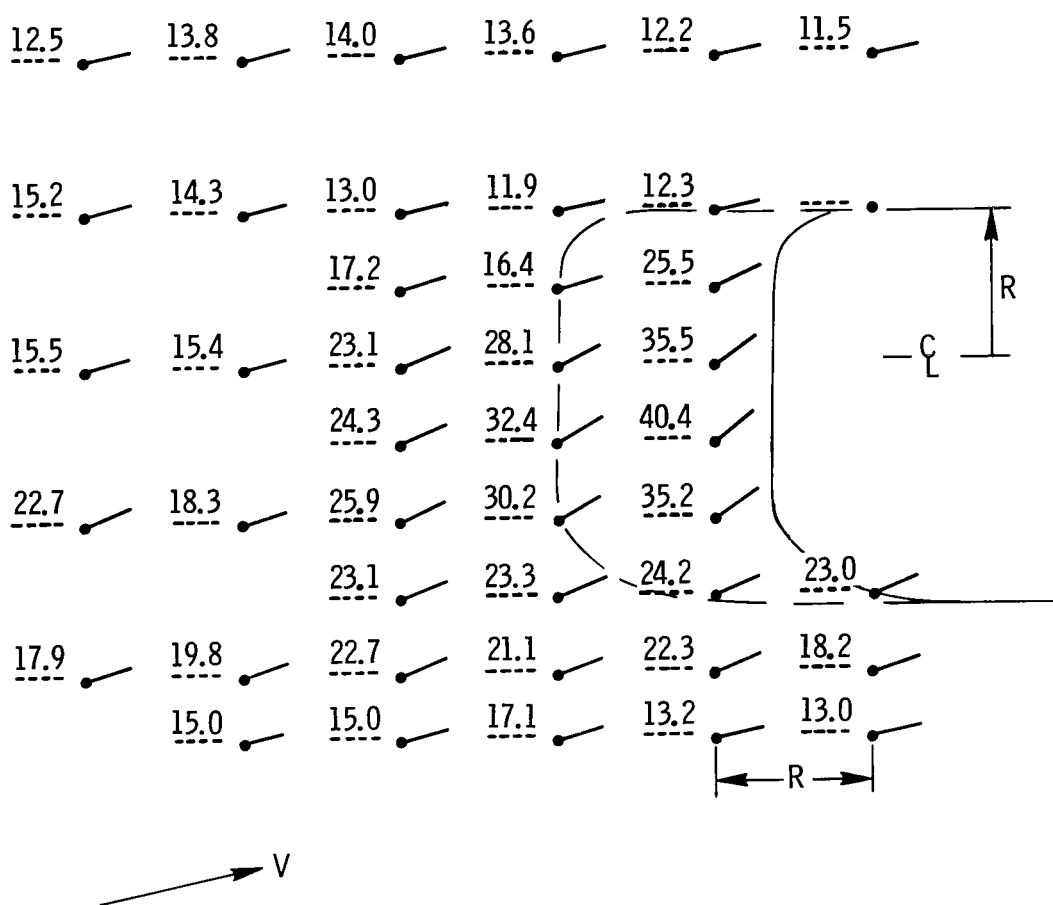
- Tufts in a chordwise plane located between the port nacelles



(a)  $\alpha = 0.5^\circ$ ;  $C_L = 2.93$ .

Figure 8.- Upflow angle, deg, between nacelles as shown by a tuft grid located at  $0.338 \frac{b}{2}$ . Flaps at  $0^\circ, 20^\circ, 40^\circ$ ;  $C_\mu = 2.0$ ; slat fillers on.

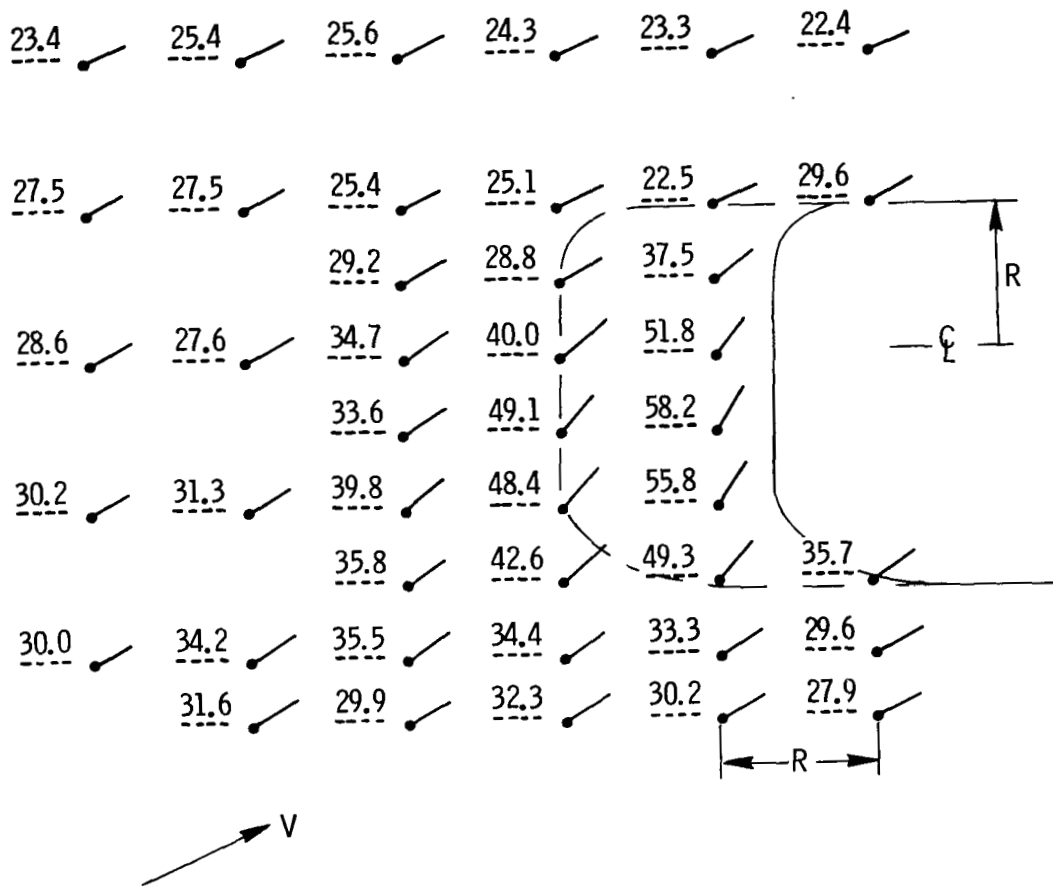
- Tufts in a chordwise plane located between the port nacelles



(b)  $\alpha = 12.7^\circ$ ;  $C_L = 5.00$ .

Figure 8.- Continued.

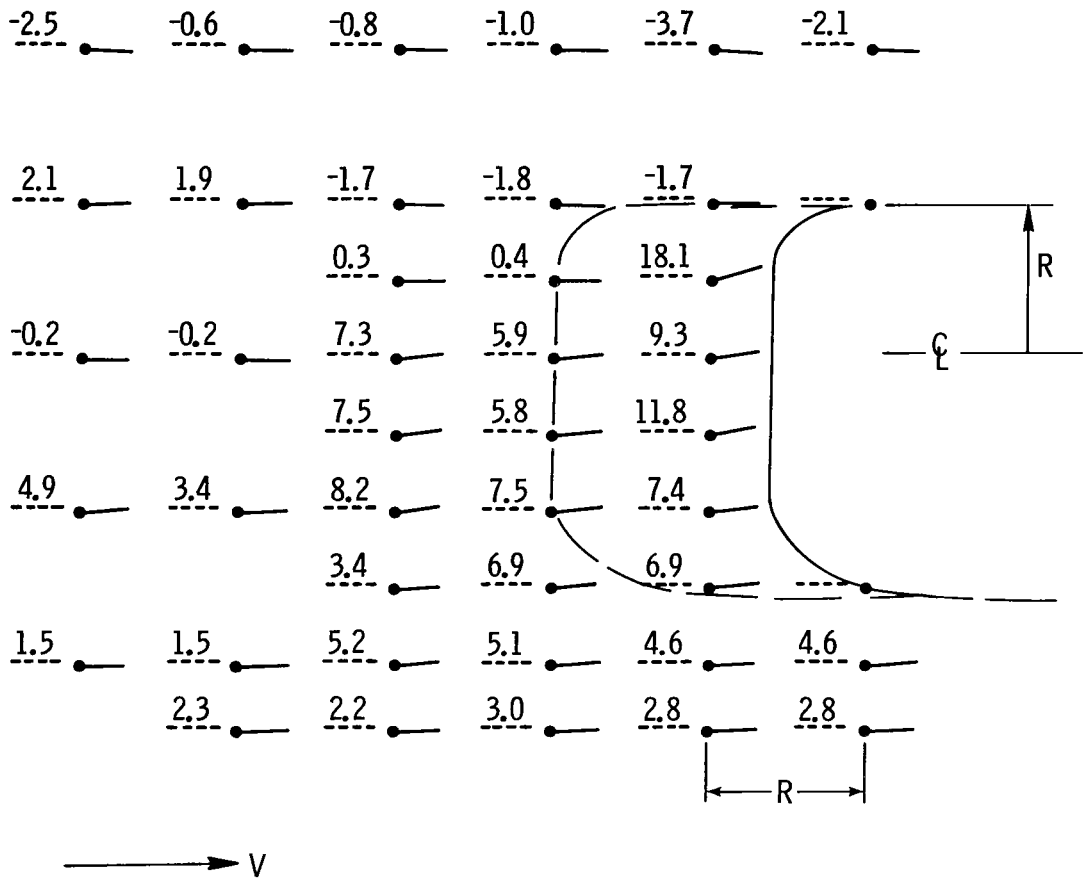
- Tufts in a chordwise plane located between the port nacelles



(c)  $\alpha = 24.8^\circ$ ;  $C_L = 6.25$ .

Figure 8.- Concluded.

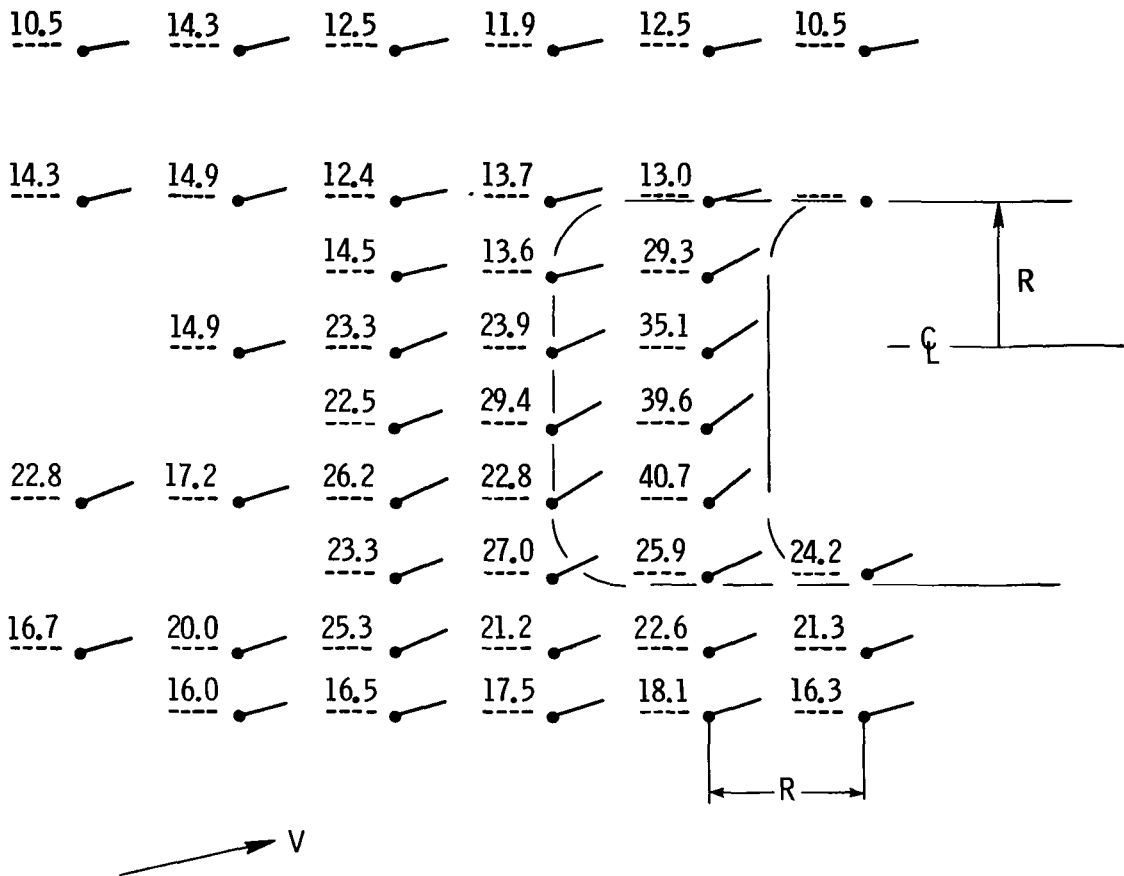
- Tufts in a chordwise plane located between the port nacelles



(a)  $\alpha = 0.6^\circ$ ;  $C_L = 3.56$ .

Figure 9.- Upflow angle, deg, between nacelles as shown by a tuft grid located at  $0.338 \frac{b}{2}$ . Flaps at  $0^\circ, 20^\circ, 40^\circ$ ;  $C_\mu = 4.0$ ; slat fillers on.

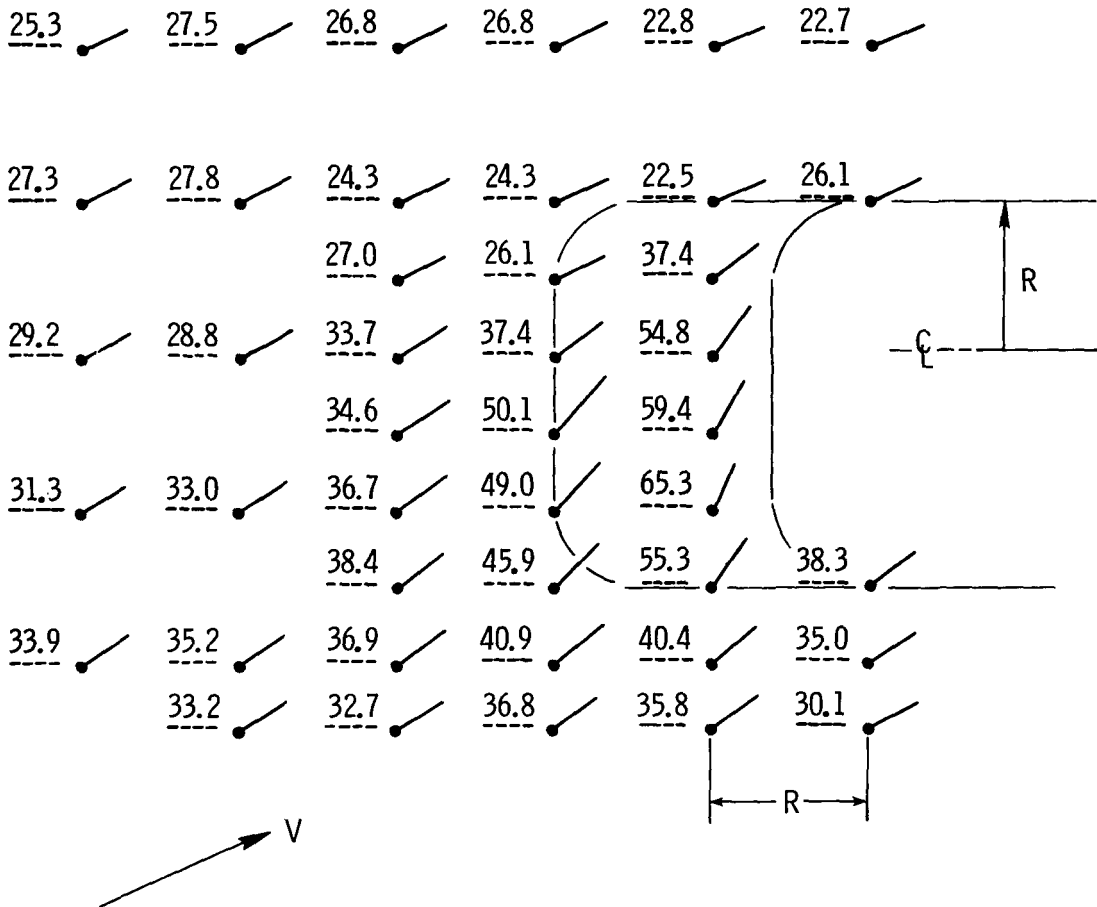
• Tufts in a chordwise plane located between the port nacelles



(b)  $\alpha = 12.7^\circ$ ;  $C_L = 5.90$ .

Figure 9.- Continued.

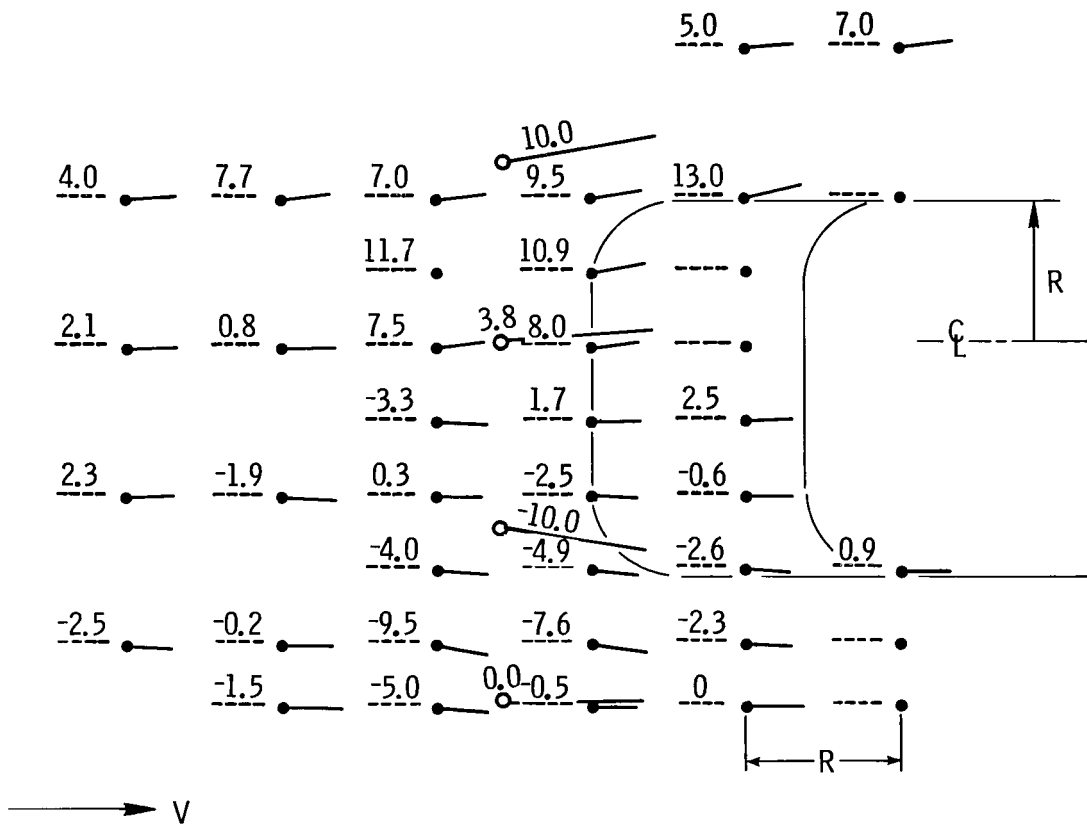
- Tufts in a chordwise plane located between the port nacelles



(c)  $\alpha = 24.8^\circ$ ;  $C_L = 7.90$ .

Figure 9.- Concluded.

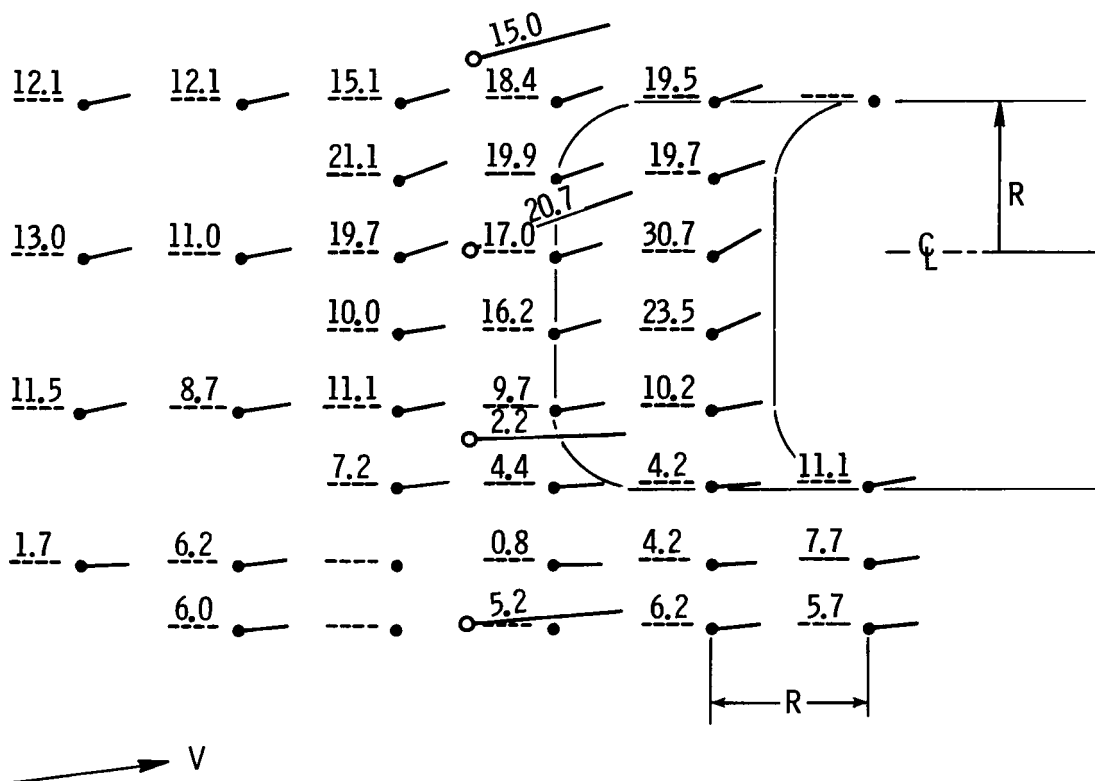
- Tufts in a chordwise plane located between the port nacelles
- Tufts in vertical plane of centerline of outboard nacelle



(a)  $\alpha = 0.5^\circ$ ;  $C_L = 2.6$ .

Figure 10.- Upflow angle, deg, between nacelles as shown by a tuft grid located at  $0.338 \frac{b}{2}$ . Flaps at  $15^\circ, 35^\circ, 55^\circ$ ;  $C_\mu = 0$ .

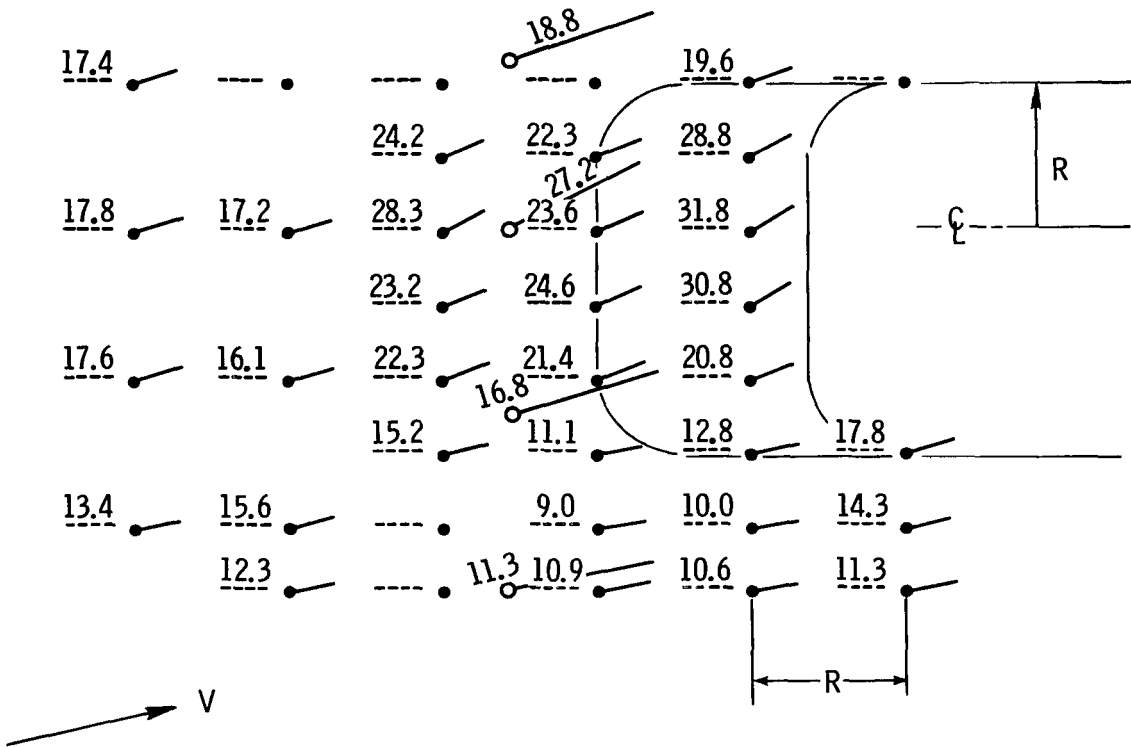
- Tufts in a chordwise plane located between the port nacelles
- Tufts in vertical plane of centerline of outboard nacelle



(b)  $\alpha = 6.7^\circ$ ;  $C_L = 3.1$ .

Figure 10.- Continued.

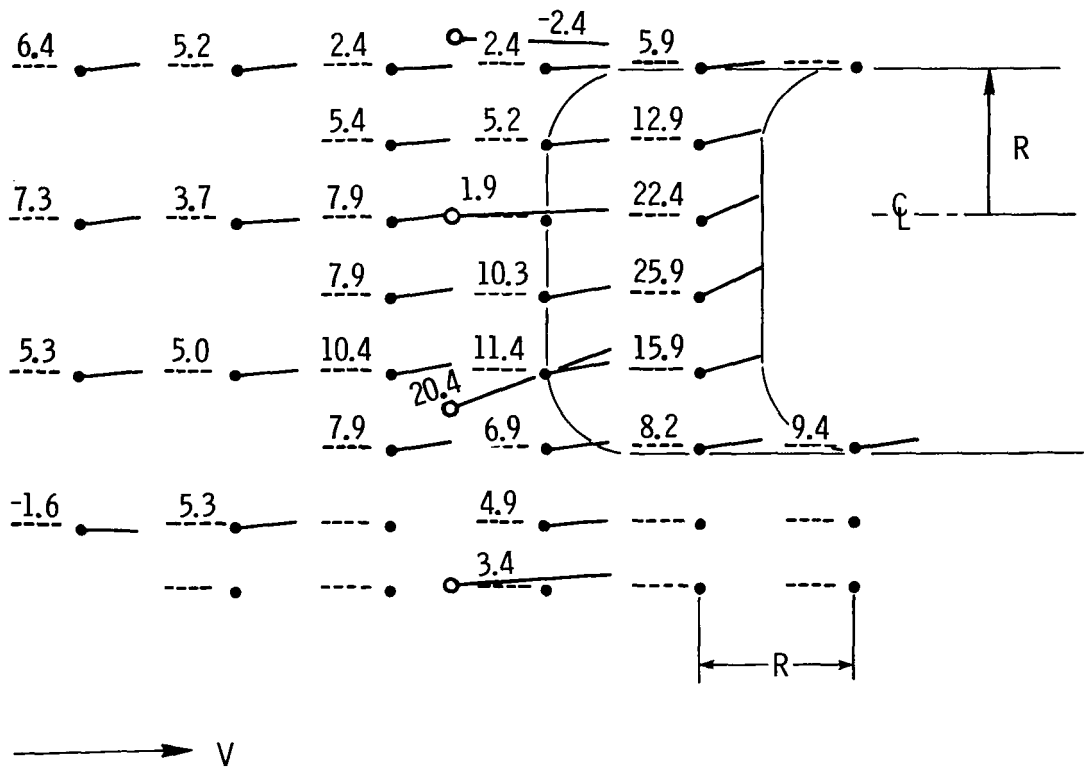
- Tufts in a chordwise plane located between the port nacelles
- Tufts in vertical plane of centerline of outboard nacelle



(c)  $\alpha = 12.8^\circ$ ;  $C_L = 2.9$ .

Figure 10.- Concluded.

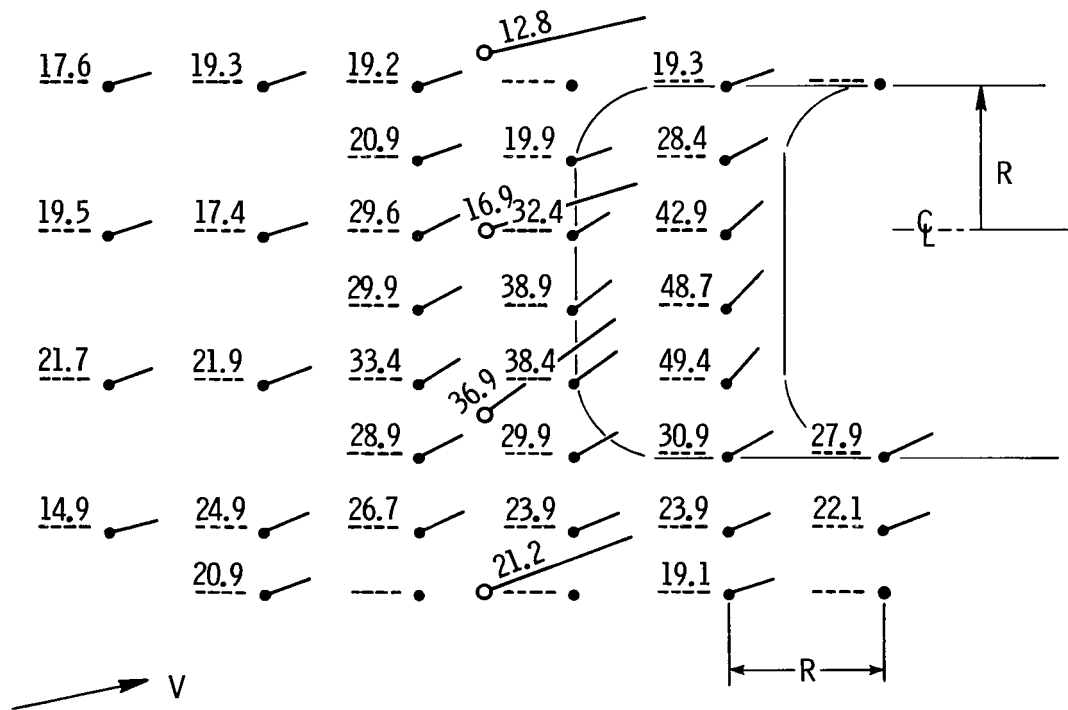
- Tufts in a chordwise plane located between the port nacelles
- Tufts in vertical plane of centerline of outboard nacelle



(a)  $\alpha = 0.9^\circ$ ;  $C_L = 4.90$ .

Figure 11.- Upflow angle, deg, between nacelles as shown by a tuft grid located at  $0.338 \frac{b}{2}$ . Flaps at  $15^\circ, 35^\circ, 55^\circ$ ;  $C_\mu = 2.0$ .

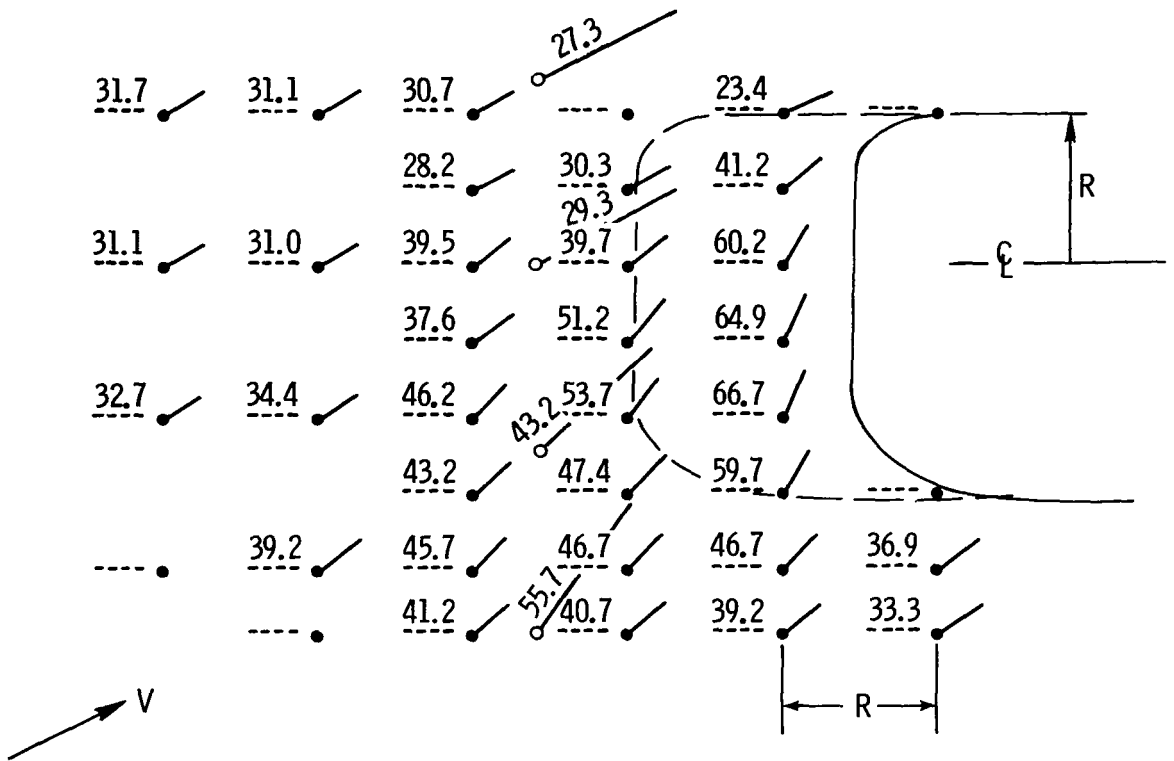
- Tufts in a chordwise plane located between the port nacelles
- Tufts in vertical plane of centerline of outboard nacelle



(b)  $\alpha = 12.4^\circ$ ;  $C_L = 6.72$ .

Figure 11.- Continued.

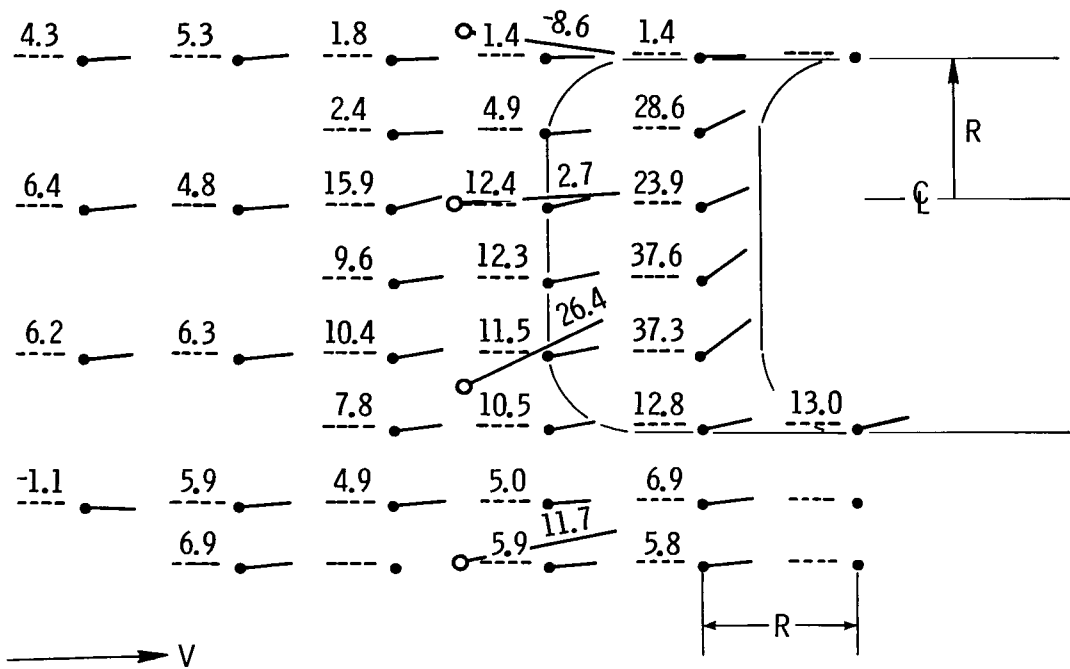
- Tufts in a chordwise plane located between the port nacelles
- Tufts in vertical plane of centerline of outboard nacelle



(c)  $\alpha = 25.7^\circ$ ;  $C_L = 6.75$ .

Figure 11.- Concluded.

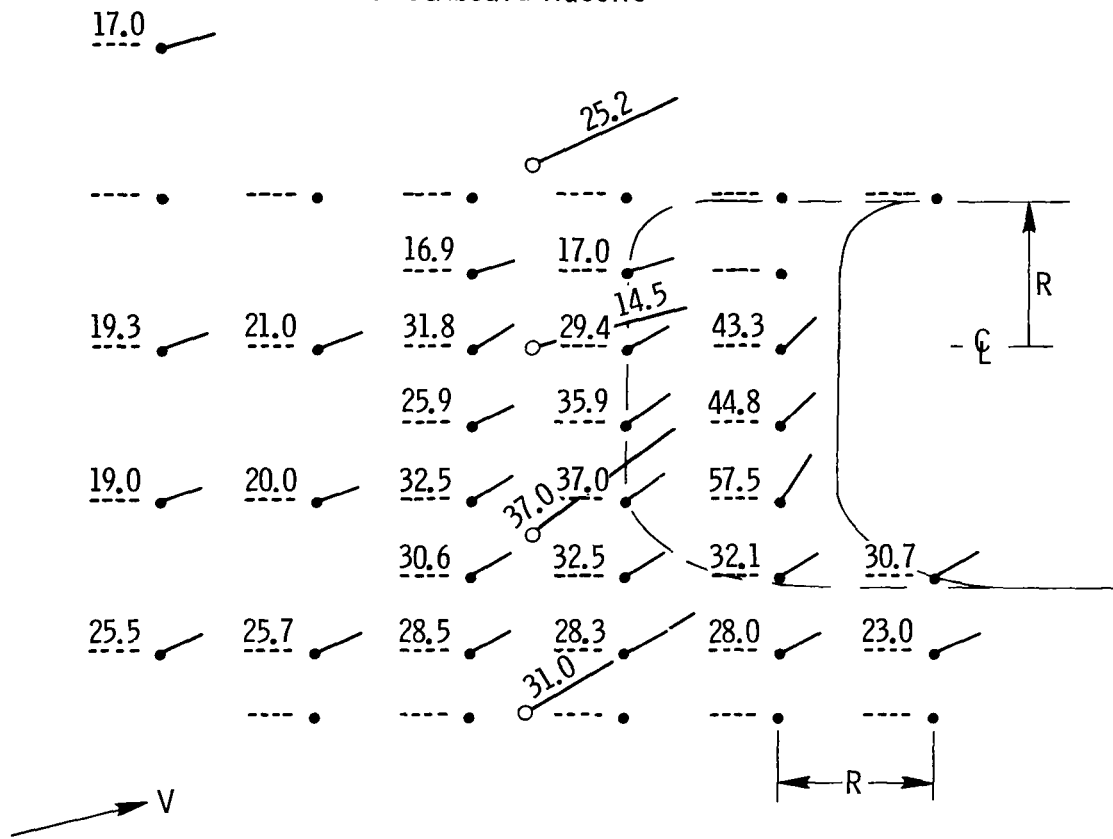
- Tufts in a chordwise plane located between the port nacelles
- Tufts in vertical plane of centerline of outboard nacelle



(a)  $\alpha = 1.4^\circ$ ;  $C_L = 6.00$ .

Figure 12.- Upflow angle, deg, between nacelles as shown by a tuft grid located at  $0.338 \frac{b}{2}$ . Flaps at  $15^\circ, 35^\circ, 55^\circ$ ;  $C_\mu = 4.0$ .

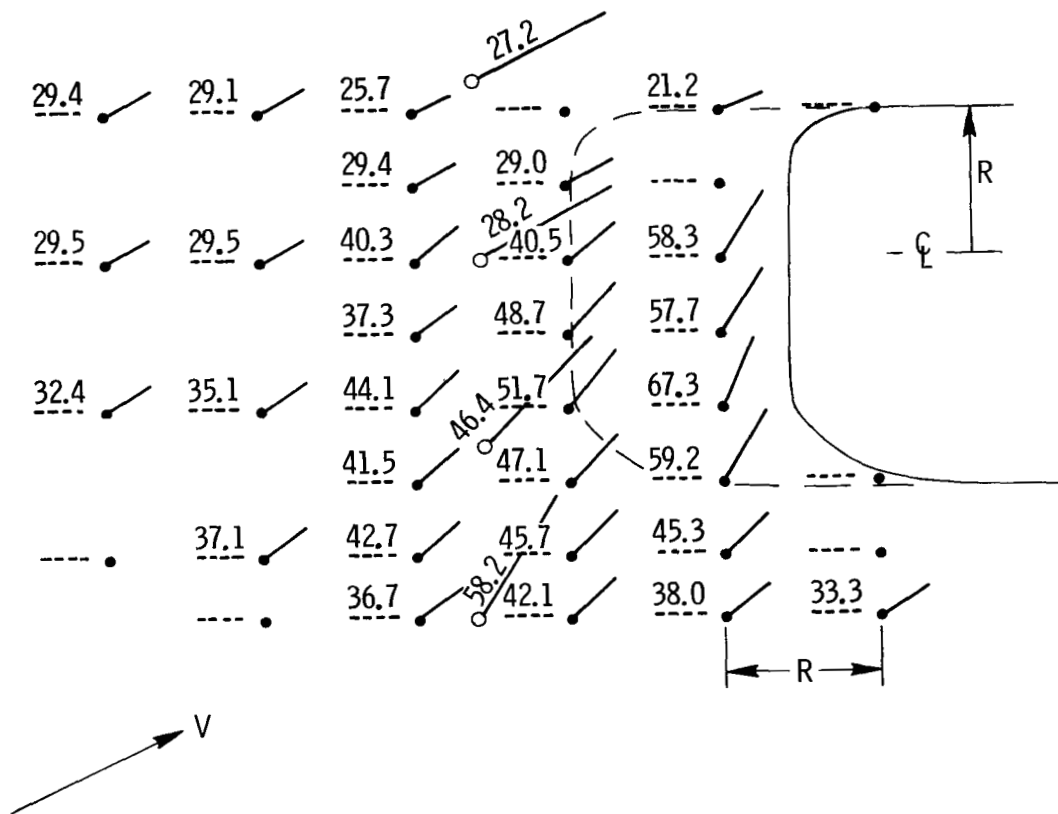
- Tufts in a chordwise plane located between the port nacelles
- Tufts in vertical plane of centerline of outboard nacelle



(b)  $\alpha = 13.5^\circ$ ;  $C_L = 8.40$ .

Figure 12.- Continued.

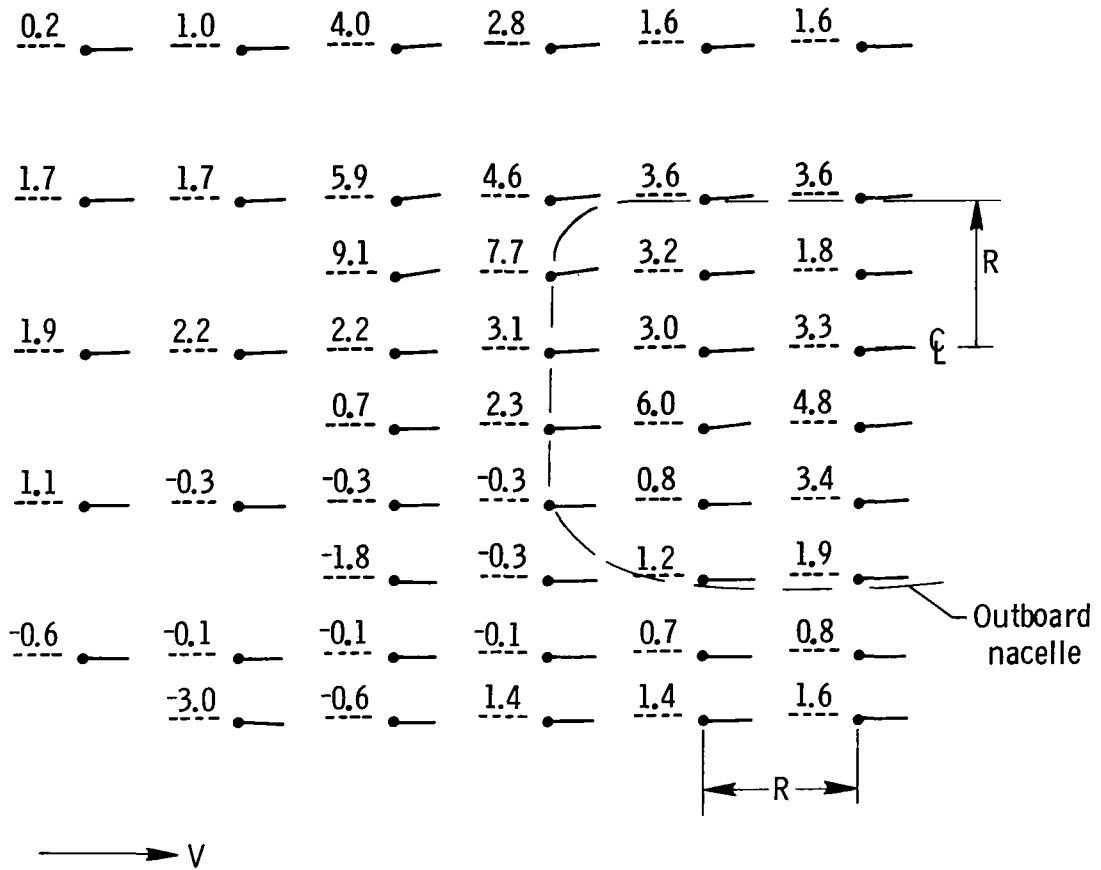
- Tufts in a chordwise plane located between the port nacelles
- Tufts in vertical plane of centerline of outboard nacelle



(c)  $\alpha = 25.7^\circ$ ;  $C_L = 9.33$ .

Figure 12.- Concluded.

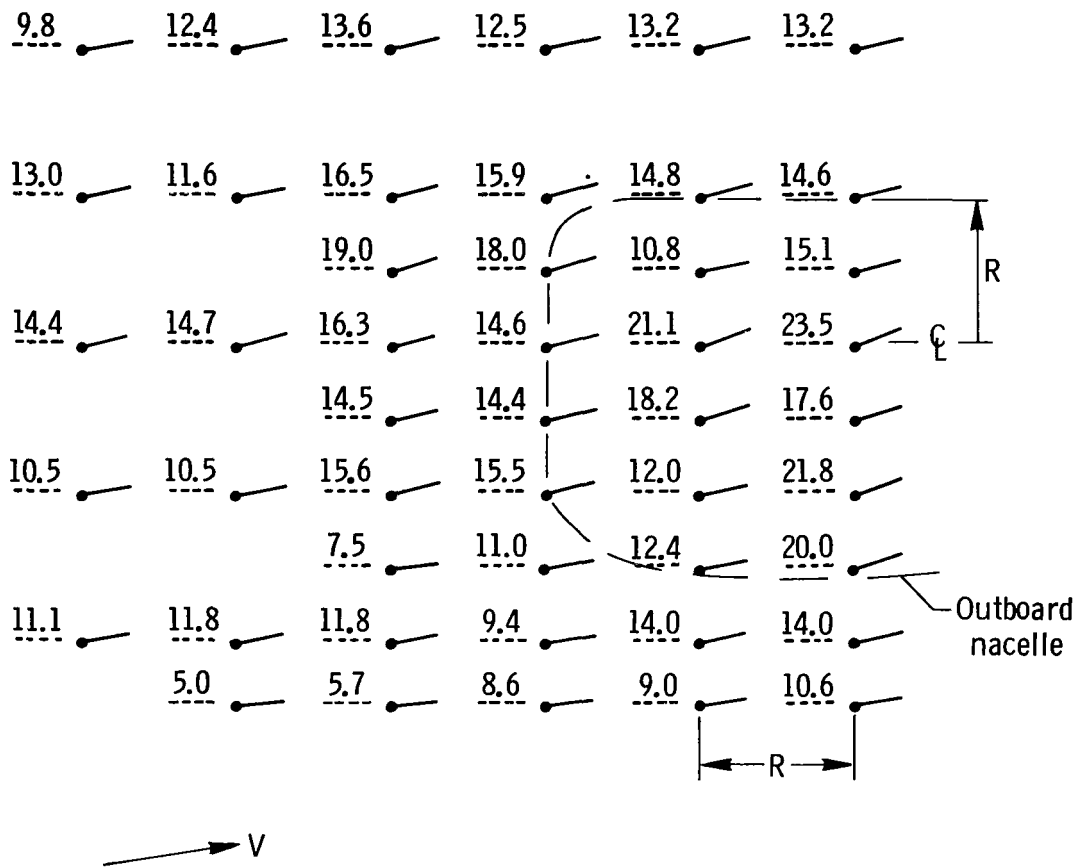
- Tufts in a chordwise plane located outboard of the port nacelles



(a)  $\alpha = -0.8^\circ$ ;  $C_L = 2.58$ .

Figure 13.--Upflow angle, deg, outboard of nacelles as shown by a tuft grid located at  $0.502 \frac{b}{2}$ . Flaps at  $15^\circ, 35^\circ, 55^\circ$ ;  $C_\mu = 0$ .

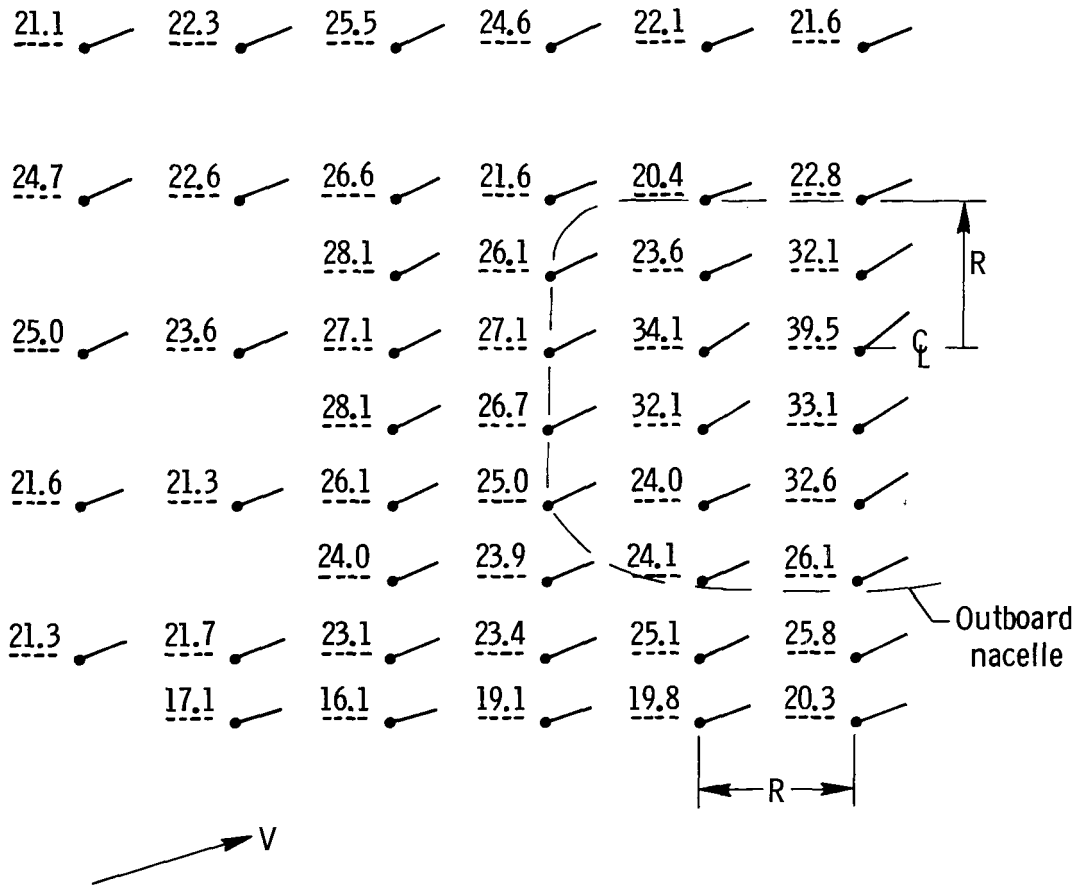
- Tufts in a chordwise plane located outboard of the port nacelles



(b)  $\alpha = 9.0^\circ$ ;  $C_L = 3.39$ .

Figure 13.- Continued.

- Tufts in a chordwise plane located outboard of the port nacelles



(c)  $\alpha = 17.1^\circ$ ;  $C_L = 3.80$ .

Figure 13.- Concluded.

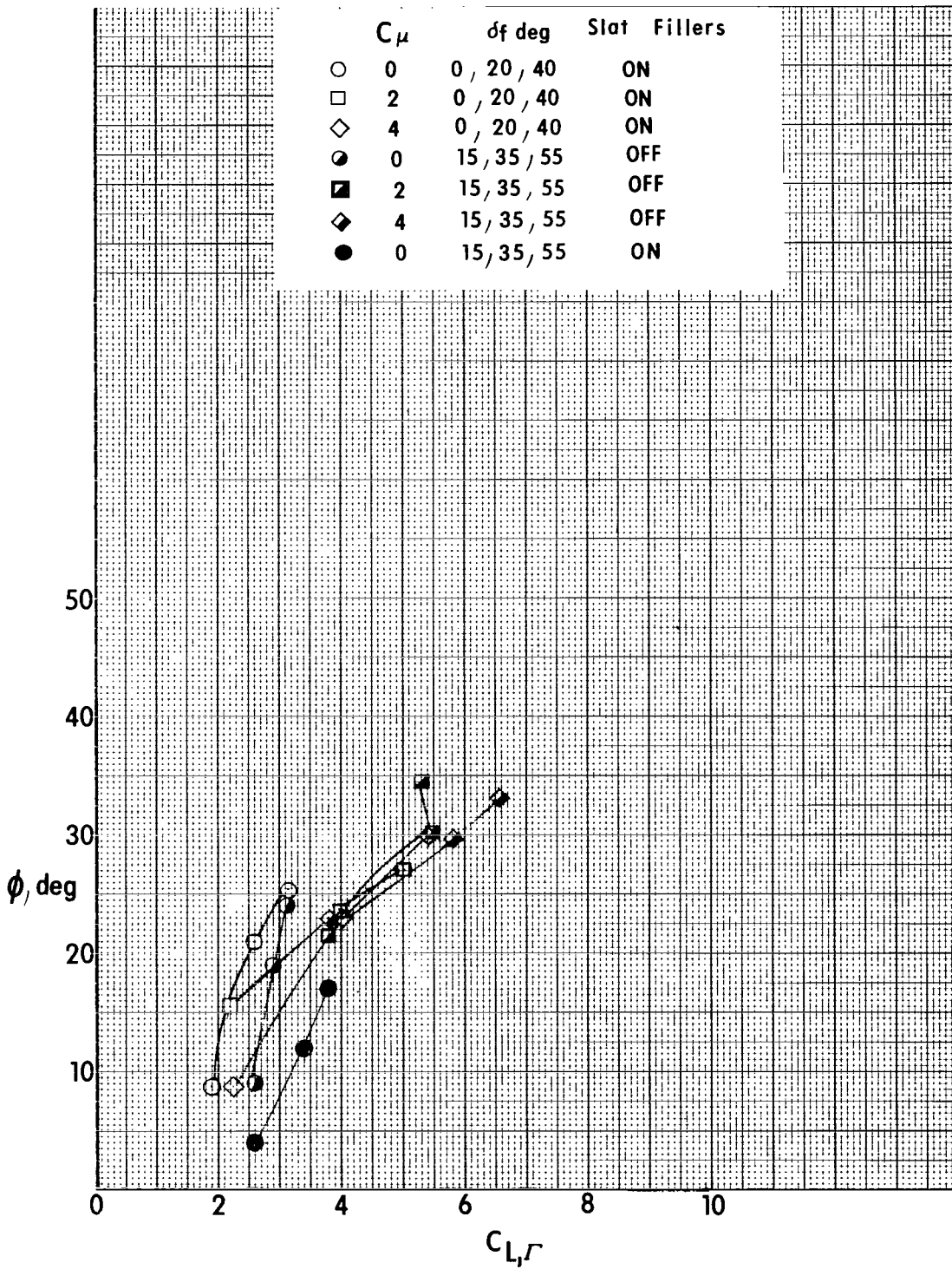
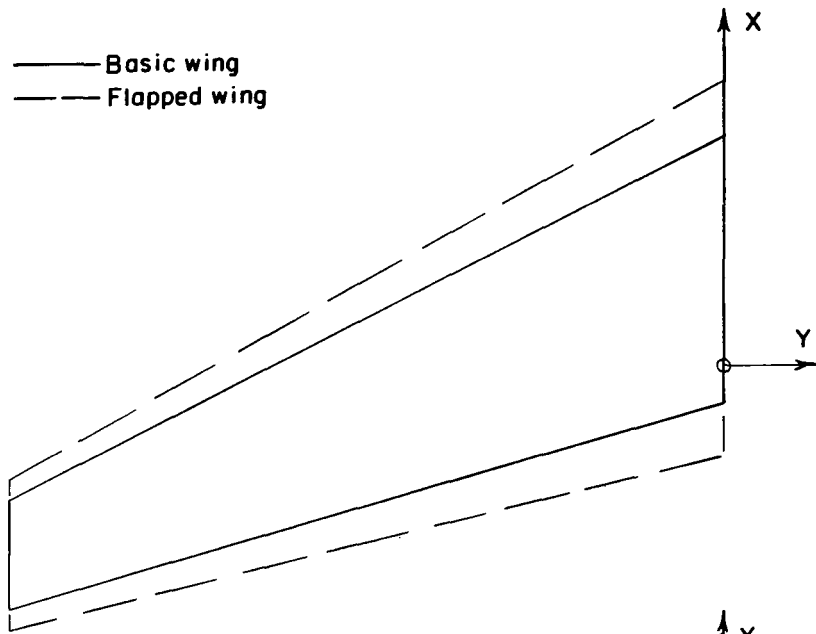
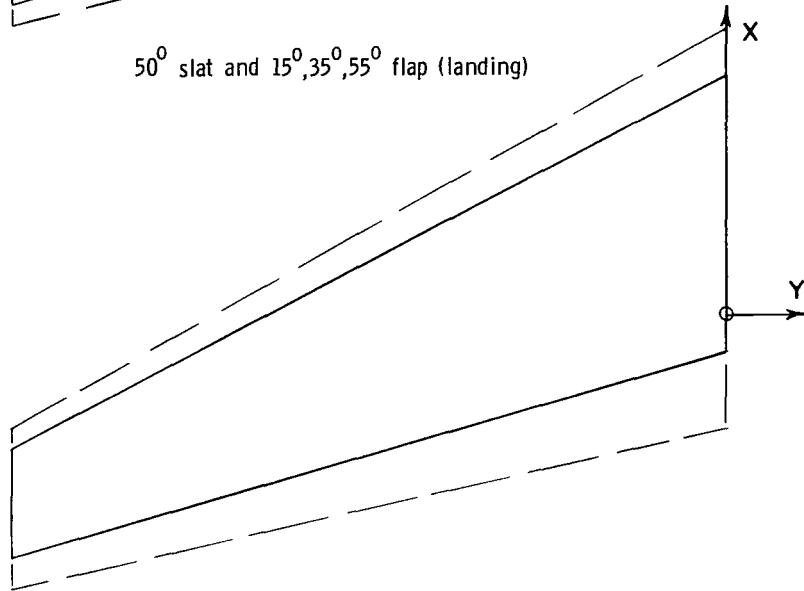


Figure 14.- Variation of upwash angle with thrust-removed lift coefficient.



50° slat and 15°, 35°, 55° flap (landing)



50° slat and 0°, 20°, 40° flap (take-off)

		PLANFORM DEFINITION POINTS			
Basic	x	32, 57(12, 82)	-17, 46(- 6, 88)	-32, 44(-12, 77)	- 4, 87(- 1, 92)
	y	0 ( 0)	-95, 25(-37, 50)	-95, 25(-37, 50)	0 ( 0)
Landing	x	39, 01(15, 36)	-14, 89(- 5, 86)	-35, 38(-13, 93)	-12, 21(- 4, 81)
	y	0 ( 0)	-95, 25(-37, 50)	-95, 25(-37, 50)	0 ( 0)
Take-off	x	39, 01(15, 36)	-14, 89(- 5, 86)	-36, 65(-14, 43)	-15, 39(- 6, 06)
	y	0 ( 0)	-95, 25(-37, 50)	-95, 25(-37, 50)	0 ( 0)

Figure 15.- Wing planforms used in calculations. Dimensions are in cm (in.).

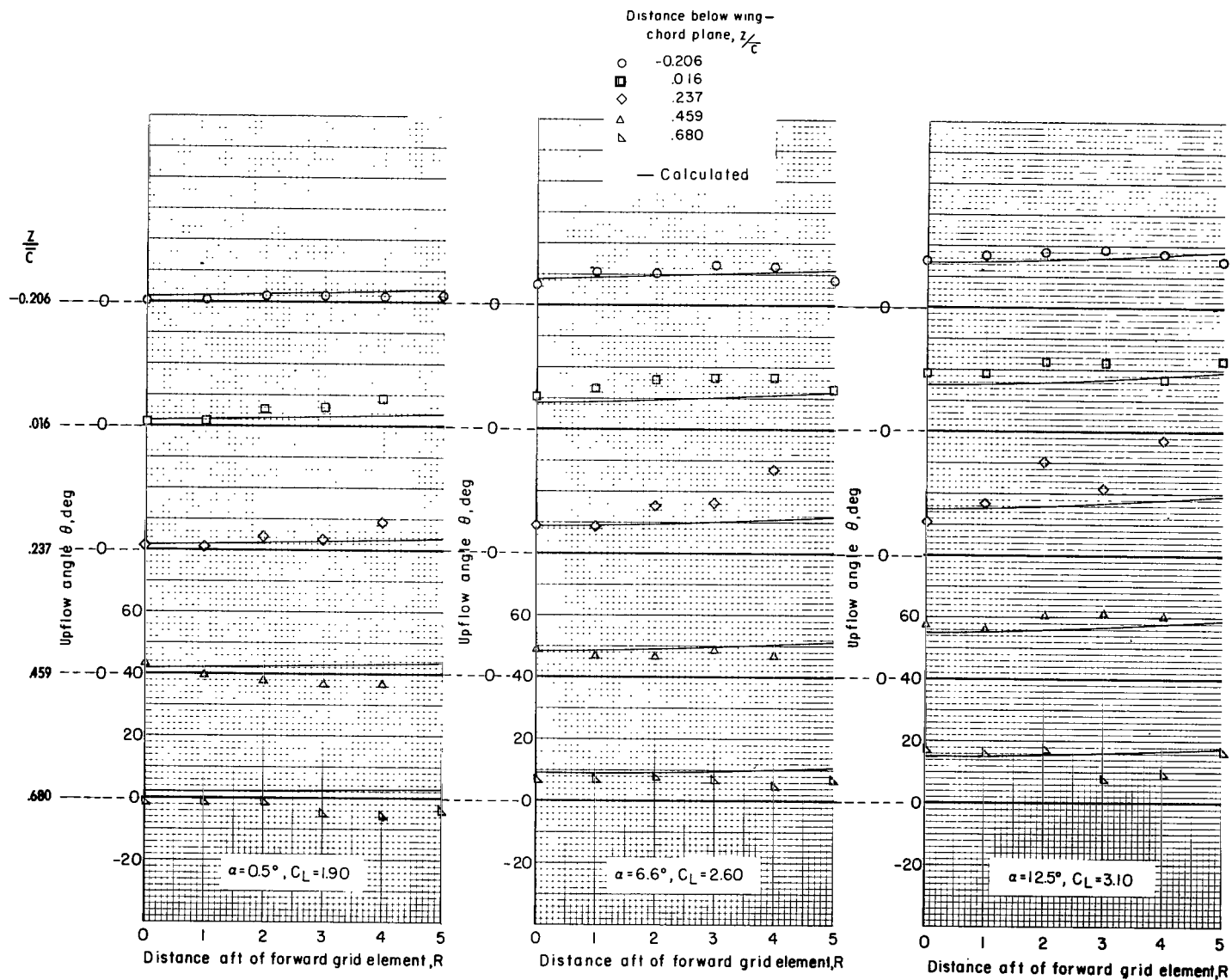


Figure 16.- Comparison of experimental and calculated flow angles; grid located between nacelles  $\left(0.338 \frac{b}{2}\right)$ ; flaps at  $0^\circ, 20^\circ, 40^\circ$ ;  $C_\mu = 0$ ; slat fillers on.

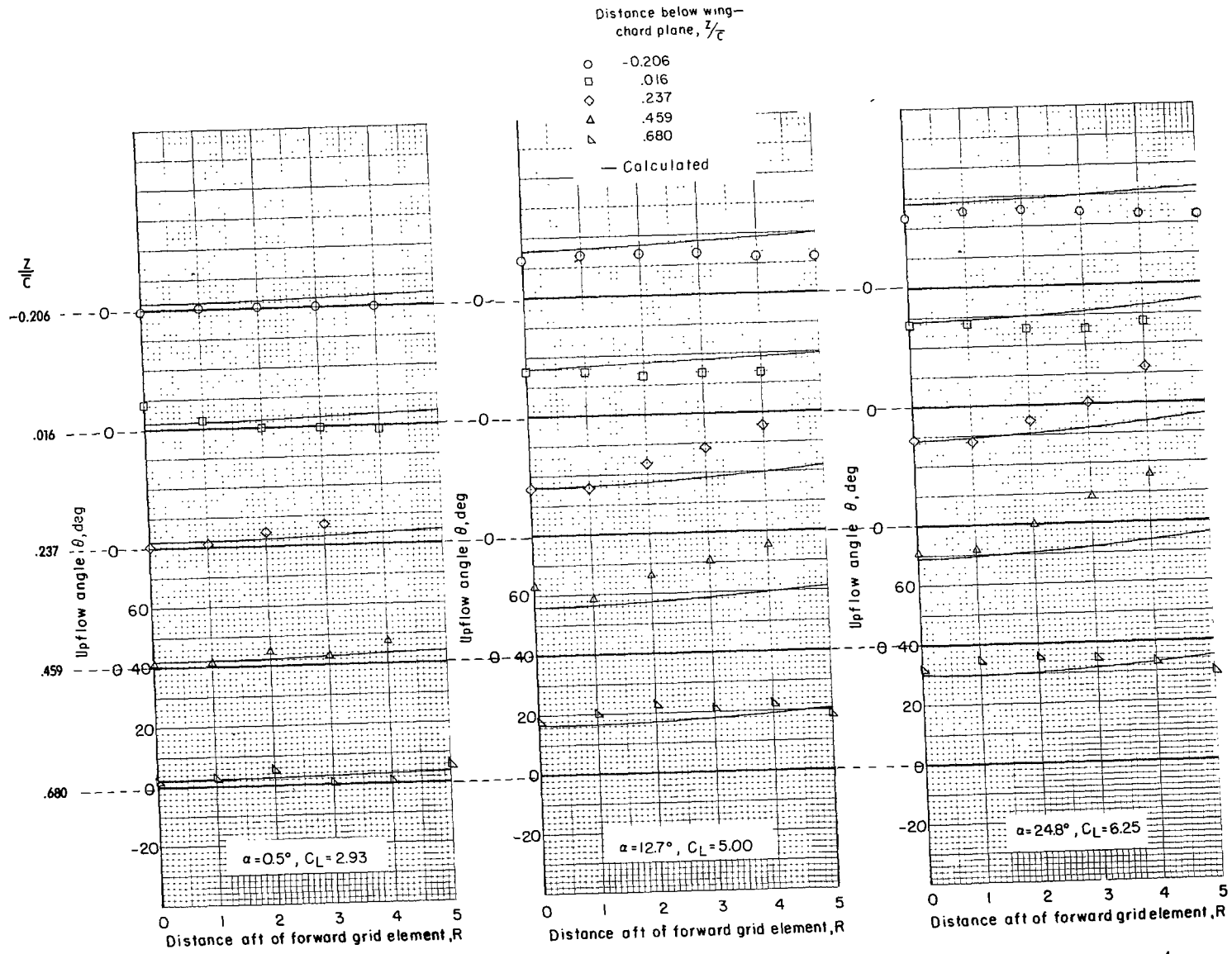


Figure 17.- Comparison of experimental and calculated flow angles; grid located between nacelles  $\left(0.338 \frac{b}{2}\right)$ ; flaps at  $0^\circ, 20^\circ, 40^\circ$ ;  $C_\mu = 2.0$ ; slat fillers on.

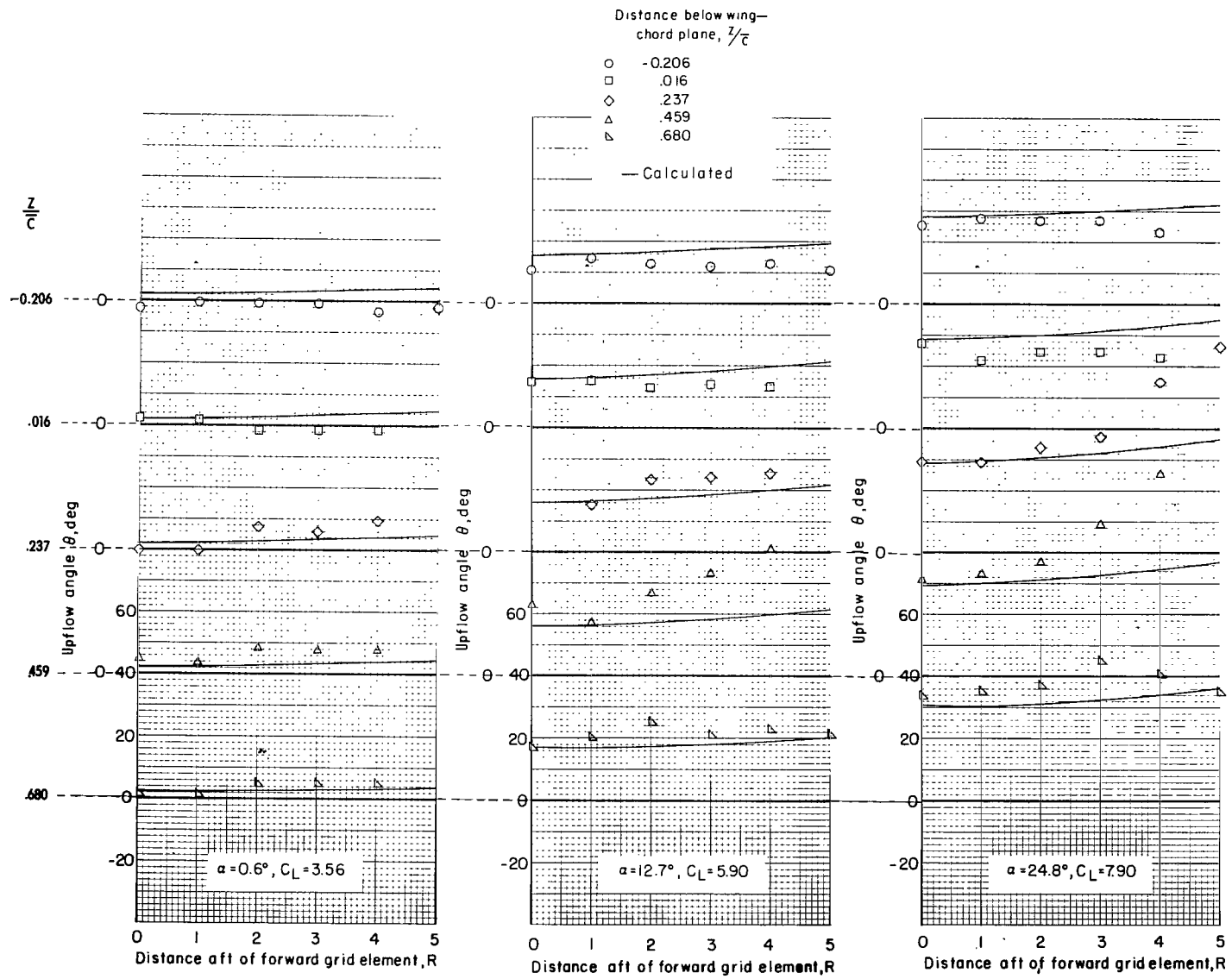


Figure 18.- Comparison of experimental and calculated flow angles; grid located between nacelles  $\left(0.338 \frac{b}{2}\right)$ ; flaps at  $0^\circ, 20^\circ, 40^\circ$ ;  $C_\mu = 4.0$ ; slat fillers on.

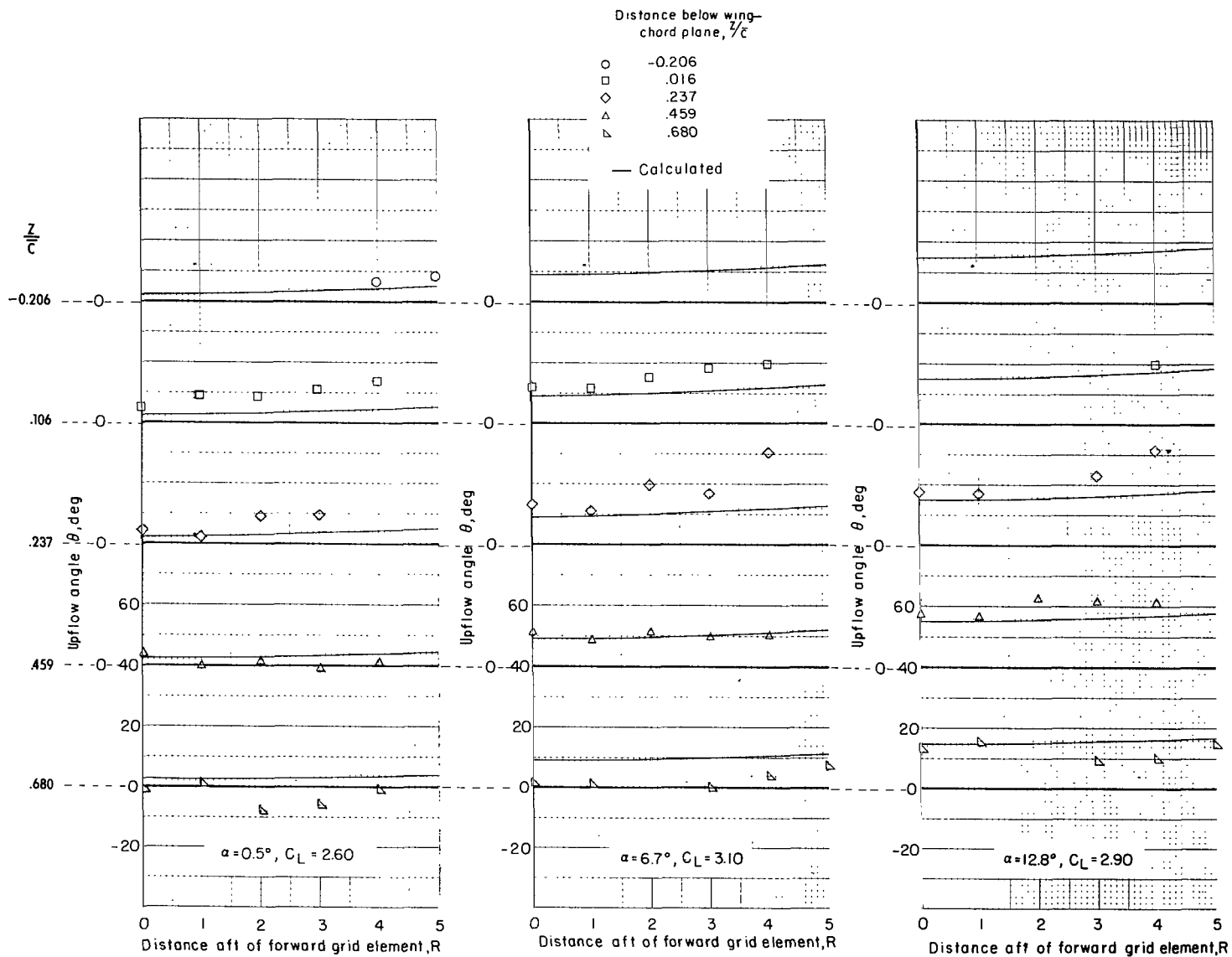


Figure 19.- Comparison of experimental and calculated flow angles; grid located between nacelles  $(0.338 \frac{b}{2})$ ; flaps at  $15^\circ, 35^\circ, 55^\circ$ ;  $C_\mu = 0$ .

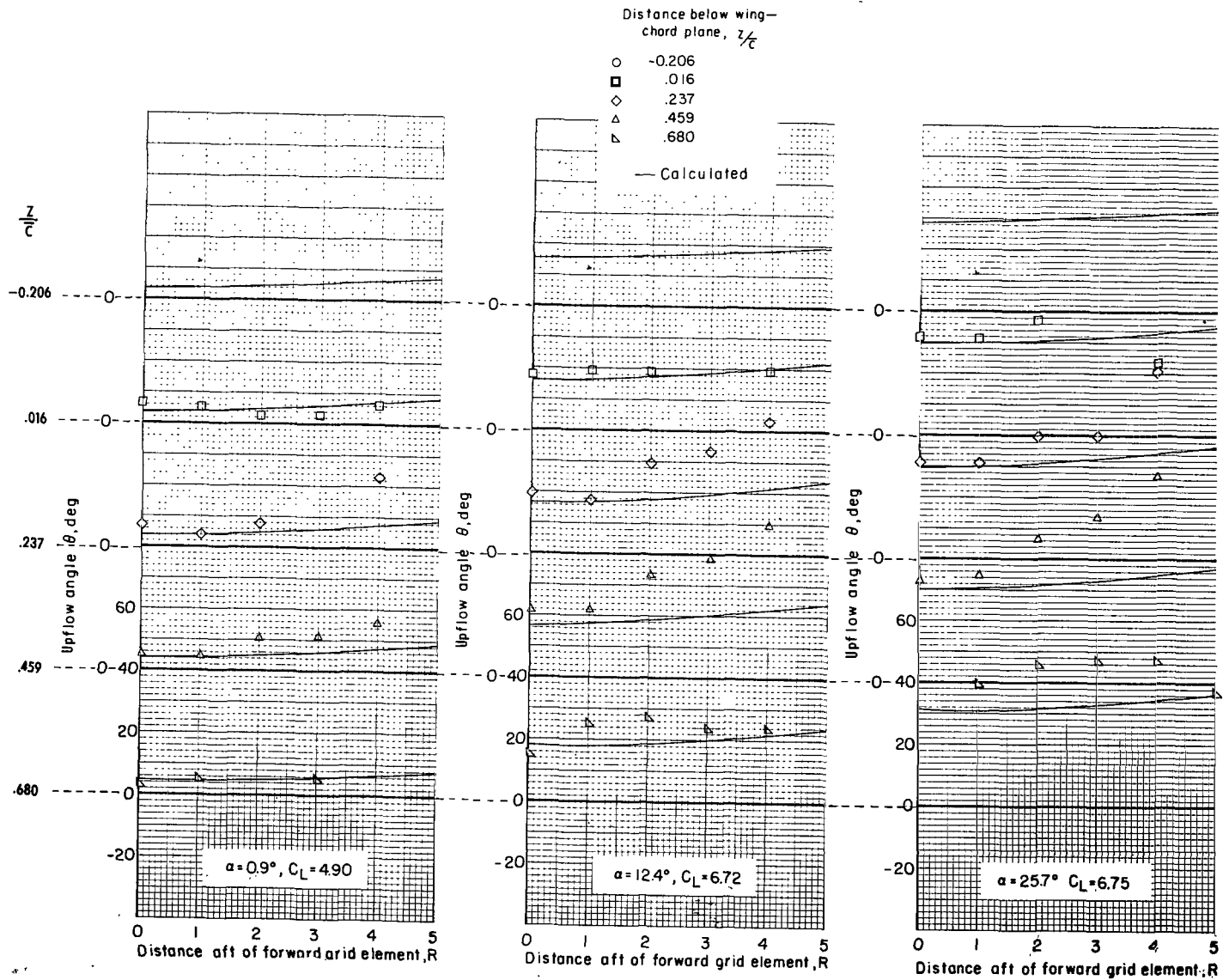


Figure 20.- Comparison of experimental and calculated flow angles; grid located between nacelles  $\left(0.338 \frac{b}{2}\right)$ ; flaps at  $15^\circ, 35^\circ, 55^\circ$ ;  $C_\mu = 2.0$ .

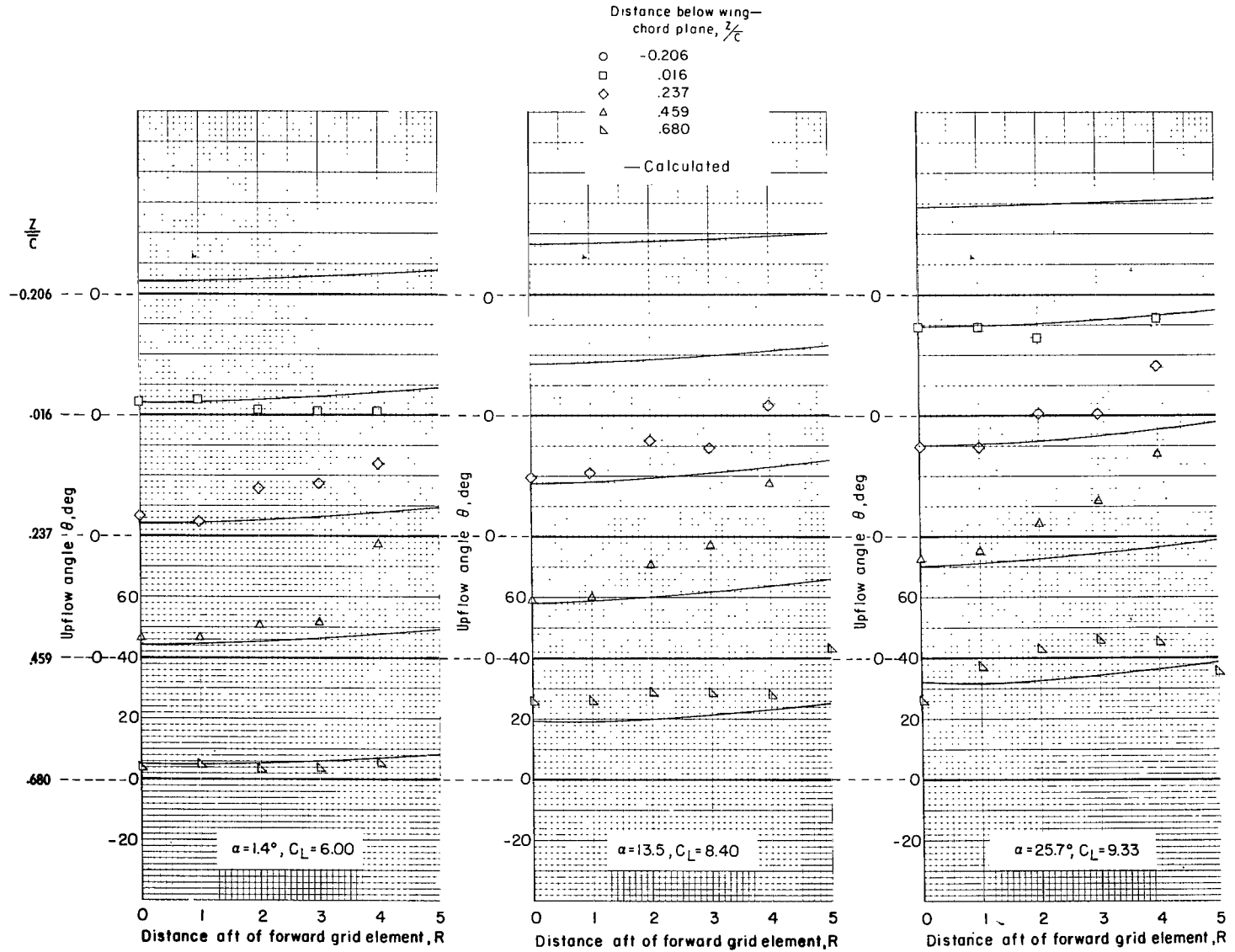


Figure 21.- Comparison of experimental and calculated flow angles; grid located between nacelles  $\left(0.338 \frac{b}{2}\right)$ ; flaps at  $15^\circ, 35^\circ, 55^\circ$ ;  $C_\mu = 4.0$ .

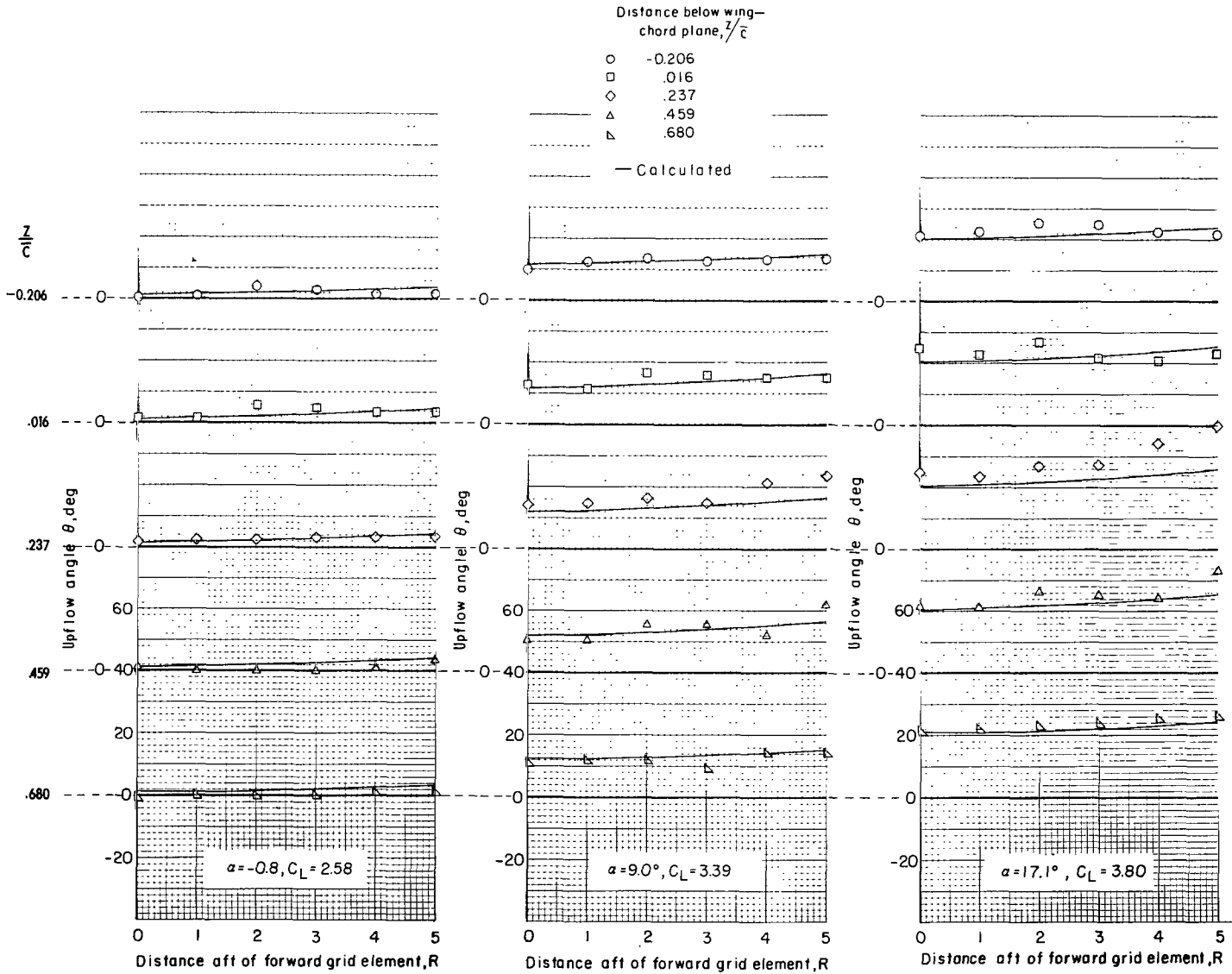


Figure 22.- Comparison of experimental and calculated flow angles; grid located at  $0.502 \frac{b}{2}$ ; flaps at  $15^\circ, 35^\circ, 55^\circ$ ;  $C_\mu = 0$ ; slat fillers on.



065 001 C1 U A 751114 S00903DS  
DEPT OF THE AIR FORCE  
AF WEAPONS LABORATORY  
ATTN: TECHNICAL LIBRARY (SUL)  
KIRTLAND AFB NM 87117

POSTMASTER: If Undeliverable (Section 158  
Postal Manual) Do Not Return

*"The aeronautical and space activities of the United States shall be conducted so as to contribute . . . to the expansion of human knowledge of phenomena in the atmosphere and space. The Administration shall provide for the widest practicable and appropriate dissemination of information concerning its activities and the results thereof."*

—NATIONAL AERONAUTICS AND SPACE ACT OF 1958

## NASA SCIENTIFIC AND TECHNICAL PUBLICATIONS

**TECHNICAL REPORTS:** Scientific and technical information considered important, complete, and a lasting contribution to existing knowledge.

**TECHNICAL NOTES:** Information less broad in scope but nevertheless of importance as a contribution to existing knowledge.

**TECHNICAL MEMORANDUMS:** Information receiving limited distribution because of preliminary data, security classification, or other reasons. Also includes conference proceedings with either limited or unlimited distribution.

**CONTRACTOR REPORTS:** Scientific and technical information generated under a NASA contract or grant and considered an important contribution to existing knowledge.

**TECHNICAL TRANSLATIONS:** Information published in a foreign language considered to merit NASA distribution in English.

**SPECIAL PUBLICATIONS:** Information derived from or of value to NASA activities. Publications include final reports of major projects, monographs, data compilations, handbooks, sourcebooks, and special bibliographies.

**TECHNOLOGY UTILIZATION PUBLICATIONS:** Information on technology used by NASA that may be of particular interest in commercial and other non-aerospace applications. Publications include Tech Briefs, Technology Utilization Reports and Technology Surveys.

*Details on the availability of these publications may be obtained from:*

**SCIENTIFIC AND TECHNICAL INFORMATION OFFICE  
NATIONAL AERONAUTICS AND SPACE ADMINISTRATION  
Washington, D.C. 20546**